A Naturally Thermolabile Activity Compromises Genetic Analysis of Telomere Function in *Saccharomyces cerevisiae*

Margherita Paschini,*,† Tasha B. Toro,*,[1] Johnathan W. Lubin,* Bari Braunstein-Ballew,*,† Danna K. Morris,‡ and Victoria Lundblad*,[2]

*Salk Institute for Biological Studies, La Jolla, California 92037-1099, †Division of Biological Sciences, University of California San Diego, La Jolla, California 92093-0130, and ‡Department of Molecular and Human Genetics, Baylor College of Medicine, Houston, Texas 77030

ABSTRACT The core assumption driving the use of conditional loss-of-function reagents such as temperature-sensitive mutations is that the resulting phenotype(s) are solely due to depletion of the mutant protein under nonpermissive conditions. However, prior published data, combined with observations presented here, challenge the generality of this assumption at least for telomere biology: for both wild-type yeast and strains bearing null mutations in telomere protein complexes, there is an additional phenotypic consequence when cells are grown above 34°. We propose that this synthetic phenotype is due to a naturally thermolabile activity that confers a telomere-specific defect, which we call the Tmp$^-$ phenotype. This prompted a re-examination of commonly used *cdc13-ts* and *stn1-ts* mutations, which indicates that these alleles are instead hypomorphic mutations that behave as apparent temperature-sensitive mutations due to the additive effects of the Tmp$^-$ phenotype. We therefore generated new *cdc13-ts* reagents, which are nonpermissive below 34°, to allow examination of *cdc13*-depleted phenotypes in the absence of this temperature-dependent defect. A return-to-viability experiment following prolonged incubation at 32°, 34°, and 36° with one of these new *cdc13-ts* alleles argues that the accelerated inviability previously observed at 36° in *cdc13-1 rad9*-Δ mutant strains is a consequence of the Tmp$^-$ phenotype. Although this study focused on telomere biology, viable null mutations that confer inviability at 36° have been identified for multiple cellular pathways. Thus, phenotypic analysis of other aspects of yeast biology may similarly be compromised at high temperatures by pathway-specific versions of the Tmp$^-$ phenotype.

TELOMERE research in the budding yeast *Saccharomyces cerevisiae* has made substantial contributions for ~30 years, starting with the cloning of yeast telomeres (Szostak and Blackburn 1982; Shampay *et al.* 1984) and the identification of the first mutant strains with altered telomere length (Carson and Hartwell 1985; Lustig and Petes 1986). Subsequent studies have identified numerous factors that contribute to yeast telomere function. Two key complexes are a telomerase complex (composed of the TLC1 RNA and the Est1, Est2, and Est3 proteins) that is responsible for elongating the G-rich strand of chromosome termini and a heterotrimeric complex that we have called the t-RPA complex (Gao *et al.* 2007), composed of the essential genes *CDC13*, *STN1*, and *TEN1*, which recruits telomerase to chromosome ends and also confers an essential protective function. In addition, numerous proteins share roles at telomeres and double-strand breaks (Tel1, the Mre11/Rad50/Xrs2 complex, and the Ku heterodimer are three examples), and a cohort of proteins negatively regulate telomere length (Rap1, Rif1, and Rif2, as well as components of DNA replication machinery). Genome-wide efforts have expanded this list with the inclusion of several hundred additional genes (Askree *et al.* 2004; Gatbonton *et al.* 2006) that impact telomere function either directly or indirectly. Collectively, this very large panel of defined mutations in known genes has been the basis for numerous *in vivo* analyses of the consequences of perturbing telomere homeostasis.

In this study, we address an additional factor that impacts chromosome termini even in wild-type yeast: the temperature

doi: 10.1534/genetics.111.137869
Manuscript received January 9, 2012; accepted for publication February 11, 2012
Supporting information is available online at http://www.genetics.org/content/suppl/2012/02/28/genetics.111.137869.DC1
[1]Present address: Sanford-Burnham Medical Research Institute, La Jolla, CA 92037.
[2]Corresponding author: Salk Institute for Biological Studies, 10010 N. Torrey Pines Rd., La Jolla, CA 92037-1099. E-mail: lundblad@salk.edu

at which cells are propagated. Compelling evidence for a temperature-induced impact on telomeres was first uncovered with the characterization of yeast strains bearing null mutations in either of the two subunits of the Ku heterodimer. Although viable at lower temperatures, *yku70*-Δ and *yku80*-Δ strains exhibit a *RAD9*-dependent terminal arrest phenotype at 36°, arresting after limited propagation as large-budded cells (Feldmann and Winnacker 1993; Feldmann *et al.* 1996; Barnes and Rio 1997). This is accompanied by a DNA damage response (Barnes and Rio 1997; Teo and Jackson 2001), arguing that cell death is due to unrepaired DNA damage although the molecular basis for inviability is a subject of some speculation (Fellerhoff *et al.* 2000; Gravel and Wellinger 2002; Smith *et al.* 2008). Regardless of the mechanism, the temperature-dependent change in the phenotype of strains bearing null mutations in the Ku heterodimer reveals a thermolabile activity which is Ku-independent. Several other observations are also consistent with a temperature-dependent contribution, as telomeres in wild-type yeast become slightly shorter when cells are propagated at 37° (Grandin and Charbonneau 2001). In addition, *est1*-Δ null strains have a more exacerbated growth defect when propagated at higher temperatures (Lundblad and Szostak 1989).

These observations suggest that the phenotype of strains with mutations in any gene affecting telomere maintenance might become more severe at higher temperatures. In this study, we systematically analyzed the contribution of temperature to the growth properties of strains bearing null mutations in two key telomere complexes (telomerase and the t-RPA complex), which has revealed a pronounced impact on growth and viability in these null mutant strains at temperatures >34°. This provides further support for a naturally occurring thermolabile activity that, when impaired at higher temperatures, gives rise to a telomere-specific phenotype, which we propose to call the **t**e**mp**erature (Tmp$^-$) phenotype. This also raises the possibility that mutations in *CDC13*, *STN1*, and *TEN1* that exhibit temperature-sensitive (ts) growth may not be ts for activity, but instead are partial loss-of-function mutations at all temperatures. Consistent with this, we present data indicating that the widely used *cdc13-1* mutation encodes a protein that is impaired for function even at the permissive temperature of 23°, rather than a thermolabile protein. Similarly, analysis of an extensive panel of *stn1*$^-$ missense mutations, including the previously isolated *stn1-13* and *stn1-63* mutations, reveals a strikingly similar phenotype: defective telomere maintenance at 23° combined with impaired growth only at temperatures >34°. We propose that this growth phenotype is due to an additive effect, as the result of a hypomorphic *stn1*$^-$ mutation combined with the Tmp$^-$ phenotype, rather than a temperature-dependent impairment of *STN1* function. A similar explanation potentially applies to a recently reported panel of *ten1*$^-$ mutations (Xu *et al.* 2009), which we surmise may also be partial loss-of-function mutations rather than ts alleles.

Numerous prior studies with the *cdc13-1* mutant strain have been performed at 36°. However, if the *cdc13-1* encodes a protein that is severely impaired at all temperatures, and if a naturally thermolabile activity further impairs function above 34°, this raises questions about phenotypic analysis of *cdc13-1* strains at 36°. We therefore generated a new panel of *cdc13-ts* mutant strains that encodes thermolabile proteins and exhibits nonpermissive temperatures from 30° to 33°, thereby allowing a reinvestigation of phenotypes in cells depleted of the Cdc13 protein under conditions where the Tmp$^-$ phenotype does not contribute. Previous analysis has indicated that *cdc13-1* strains rapidly become inviable following incubation at 36° through a *RAD9*-dependent mechanism. However, when this experiment was repeated with one of the newly isolated *cdc13-ts* strains, loss of viability in the absence of *RAD9* was minimal at the fully nonpermissive temperature of 32° and became substantial only at 34°–36°. This indicates that inviability is the combined consequence of three defects (in *CDC13*, *RAD9*, and the thermosensitive activity) and further suggests that analysis of phenotype(s) of *cdc13-ts* strains at ≥34° may be monitoring defect(s) that are not solely attributable to loss of *CDC13* function.

Materials and Methods

Yeast strains and plasmids

All yeast strains, described in Table 1, were isogenic. Integrated alleles of *CDC13* and *STN1* were introduced into the genome as *URA3* pop-in integrants, Ura$^-$ "pop-outs" were selected on 5-FOA, and the status of the *CDC13* or *STN1* locus was assessed by PCR and sequencing to confirm that the relevant mutation was correctly integrated. A list of the plasmids as well as the starting vectors used for each set of plasmid constructions are in Tables 2 and 3.

Genetic methods

Standard genetic methods (telomere length analysis, tetrad dissection, plasmid shuffle, viability assays, and flow cytometry) were performed as previously described (Lendvay *et al.* 1996; Paschini *et al.* 2010). For senescence assays, the relevant diploid strains were dissected, and the growth characteristics of *tlc1*-Δ strains were analyzed by three successive streak-outs on rich media and scored for growth after 3 days. This assay employed very large numbers of isolates to address the high degree of variability displayed by telomerase-defective strains undergoing senescence; senescence was also assessed genotype-blind for the analysis shown in Figure 8 (see Gao *et al.* 2010 for a more detailed discussion of this protocol).

Mutagenesis protocols

Two forward mutagenesis screens of *CDC13* were conducted. In the first, pVL440 (containing the intact *CDC13* gene) was propagated in an *Escherichia coli* mutator strain as described

Table 1 Strains used in this study

Strain	Genotype
JB811	*MAT***a** *leu2 trp1 ura3-52 prb*$^{-}$ *prc*$^{-}$ *pep4-3*
YVL3006	*MATα cdc13-Δ::LYS2 ura3*-52 *lys2*-801 *trp1*-Δ1 *his3*-Δ200 *leu2*-Δ1/pVL438
YVL2394	*MAT***a** *stn1-Δ::kanMX6 ura3-52 lys2*-801 *trp1*-Δ1 *his3*-Δ200 *leu2*-Δ1 *ade2*-101/p1046
YVL3584[a]	*MAT***a/α** *tlc1-Δ::HIS3/TLC1*
YVL3621[a]	*MAT***a/α** *tlc1-Δ::HIS3/TLC1 cgi1121-Δ::kanMX6/CGI121 ade2*-101/*ade2*-101
YVL2004[a]	*MAT***a/***MATα cdc13-Δ::LYS2/CDC13 rad24-Δ::HIS3/RAD24 ade2*-101/*ade2*-101
YVL3644[a]	*MAT***a/***MATα cdc13-Δ::LYS2/CDC13 rad24-Δ::HIS3/RAD24 ade2*-101/*ade2*-101 *cgi1121-Δ::cNAT/CGI121*
YVL2005[a]	*MAT***a/***MATα cdc13-Δ::LYS2/CDC13 rad17-Δ::HIS3/RAD17 ade2*-101/*ade2*-101
YVL2060[a]	*MAT***a/***MATα cdc13-Δ::LYS2/CDC13 mec3-Δ::kanMX6/MEC3 ade2*-101/*ade2*-101
YVL2072[a]	*MAT***a/***MATα cdc13-Δ::LYS2/CDC13 rad50-Δ::kanMX6/RAD50 ade2*-101/*ade2*-101
YVL2090[a]	*MAT***a/***MATα stn1-Δ::kanMX6/STN1 rad24-Δ::HIS3/RAD24 ade2*-101/*ade2*-101
YVL2091[a]	*MAT***a/***MATα ten1-Δ::kanMX6/TEN1 rad24-Δ::HIS3/RAD24 ade2*-101/*ade2*-101
YVL3461[a]	*MAT***a/***MATα stn1-I73A/STN1*
YVL3463[a]	*MAT***a/***MATα stn1-I73S/STN1*
YVL3474[a]	*MAT***a/***MATα stn1-G137A/STN1*
YVL3470[a]	*MAT***a/***MATα stn1-G137S/STN1*
YVL3658[b]	*MAT***a** *cdc13-S611L*
YVL3660[b]	*MAT***a** *cdc13-F684S*
YVL3662[b]	*MAT***a** *cdc13-S531F*
YVL3664[b]	*MAT***a** *cdc13-N609A*
YVL3666[b]	*MAT***a** *cdc13-F683L*
YVL3806[b]	*MAT***a** *cdc13-S611L rad9-Δ::kanMX6*

[a] Additional genotype: *ura3*-52/*ura3*-52 *lys2*-801/*lys2*-801 *trp1*-Δ1/*trp1*-Δ1 *his3*-Δ200/*his3*-Δ200 *leu2*-Δ1/*leu2*-Δ1.
[b] Additional genotype: *bar1-Δ::cNAT ura3-52 lys2-801 trp-Δ1 his3-Δ200 leu2-Δ1*.

previously (Bertuch and Lundblad 2003) to generate a mutant library of 17,000 plasmids, which was transformed into YVL3006 (a *cdc13*-Δ/p *CDC13 URA3* shuffle strain). Transformants were subsequently screened for viability at 23° and 36° by replica-plating onto 5-FOA-containing media. In the second screen, a DNA fragment encompassing the DNA-binding domain (DBD) of Cdc13 (amino acids 452–694) was subjected to PCR under error-prone conditions in the presence of 10 mM $MnCl_2$ and one-by-one limiting concentrations of each of the four dNTPs. Pooled PCR products were cotransformed with pVL440 gapped by digestion with *Bam*HI and *Nru*I into the *cdc13*-Δ/p *CDC13 URA3* shuffle strain. The resulting 30,000 yeast transformants bearing the gap-repaired plasmids were screened for viability at 23°, 30°, and 36° by replica-plating onto 5-FOA-containing media. For both screens, candidate plasmids were rescued, retransformed to confirm the ts phenotype and subsequently sequenced. Residues for reverse mutagenesis were selected by submitting the Cdc13 DBD or the Stn1 N-terminal OB-fold (oligosaccharide/oligonucleotide binding) domain to the Evolutionary Trace server (http://pdbjets.protein.osaka-u.ac.jp/); residues ranked in the top 10% (for Cdc13) or the top 20 residues (for Stn1) were chosen for mutagenesis.

Table 2 Plasmids used in this study

Plasmid	Description	Vector backbone
pVL438	*CEN URA3 CDC13*	
pVL440	*CEN LEU2 CDC13*	
pVL1086	*CEN LEU2 CDC13-(myc)$_{18}$*	
pVL4222	*CEN LEU2 cdc13-1-(myc)$_{18}$*	
pVL439	*URA3 CDC13*	
pVL1492	*CEN LEU2 STN1*	YCplac111
pVL4919	*CEN LEU2 stn1-63*	YCplac111
pVL4330	*CEN LEU2 STN1-(G)$_9$-(myc)$_7$*	pVL1492
pVL4992	*CEN LEU2 stn1-63-(G)$_9$-(myc)$_7$*	pVL4330
pVL4951	*URA3 stn1-I73A*	YIplac211
pVL4952	*URA3 stn1-I73S*	YIplac211
pVL4958	*URA3 stn1-G137A*	YIplac211
pVL4956	*URA3 stn1-G137S*	YIplac211

Results

Telomere-shortening activities are enhanced at 36° in wild-type S. cerevisiae

A number of prior studies have indicated that telomere function is impaired by growth at 36°–37°, including even telomere length in wild-type yeast (Grandin and Charbonneau 2001). We re-investigated the effect of temperature on telomere length by propagating two wild-type haploid strains (which were *MATα* or *MAT***a** but otherwise isogenic) in

Table 3 New temperature-sensitive mutations in *CDC13*

	Parental plasmids		
Mutation	pVL440	pVL1086	pVL439
cdc13-F684S	pVL3945	pVL5156	pVL5439
cdc13-S531F	pVL3948	pVL5157	pVL5440
cdc13-F683L	pVL3943	pVL5155	pVL5453
cdc13-N609A	pVL3956	pVL5158	pVL5441
cdc13-S611L	pVL3939	pVL5154	pVL5438

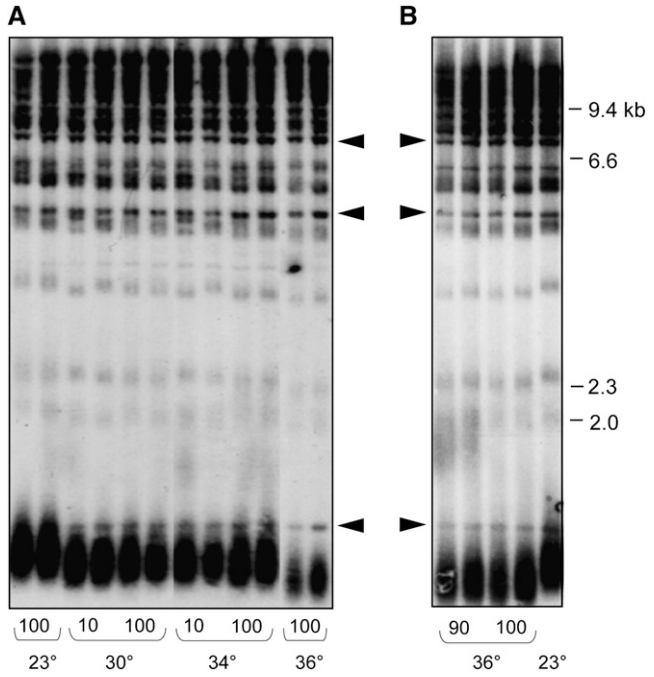

Figure 1 Telomere length in wild-type *S. cerevisiae* is temperature-sensitive. (A) Each haploid strain was propagated for ~100 generations by successive serial dilution of duplicate cultures at the indicated temperatures and genomic DNA prepped for telomere length analysis; two exposures were used to assemble the image to ensure equivalent signal intensity for each lane (as evaluated by comparison of nontelomeric bands, indicated by arrowheads). (B) The same experiment as in A, with samples from 90- and 100-generation cultures grown at 36° displayed immediately adjacent to a sample grown at 23°.

liquid culture at 23°, 30°, 34°, and 36° for ~100 generations. Comparison of telomere length showed that the samples grown at 30° and 34° underwent a very slight decline in telomere length, relative to the length displayed by the same cultures that had been propagated at 23° (Figure 1A). This change in telomere length homeostasis was reached within 10 generations of growth, with no further length decline upon extended propagation at the higher temperature. At 36°, telomeres underwent a further decline in length, so that the difference in length between cultures grown at 23° *vs.* 36° was clearly evident (Figure 1B).

There are two possible explanations for this temperature-dependent effect on telomere length: (i) elongation of telomeres by telomerase is impaired at higher temperatures or (ii) one or more processes that actively shorten telomeres is enhanced at higher temperatures. To distinguish between these two possibilities, the senescence phenotype of a telomerase null strain propagated at 23°, 30°, 32°, 34°, and 36° was examined by successive streak-outs at each temperature, following dissection of a *TLC1*/*tlc1*-Δ diploid strain. Senescence was assessed by monitoring the growth characteristics of a large number of isolates to overcome the variability of the senescence phenotype displayed by telomerase-defective strains (Rizki and Lundblad 2001; Gao *et al.* 2010). Figure 2A compares the growth characteristics of 42 *tlc1*-Δ isolates grown at 23° *vs.* 36° for three successive streak-outs, which demonstrates that the senescence progression was clearly exacerbated by growth at 36° even by the second set of streak-outs (which corresponds to ~50 generations of growth). The histogram in Figure 2B, which summarizes the relative change in the senescence score at 30°, 34°, and 36° relative to 23°, shows that senescence is also accelerated at 30° and 34°, although not to the same degree as at 36°. Thus, at higher temperatures, telomeres are shorter in the presence of telomerase, and senescence is enhanced in the absence of telomerase, which is consistent with the premise that some process by which telomeres are shortened is more active at 34° to 36° (the Tmp$^-$ phenotype). We therefore propose that the growth characteristics of the *tlc1*-Δ strain at elevated temperatures is due to the combined result of the Est$^-$ (**e**ver **s**horter **t**elomeres) and Tmp$^-$ phenotypes.

Microcolony growth of cdc13-Δ rad24-Δ and stn1-Δ rad24-Δ strains is reduced at 34°–36°

Although *cdc13*-Δ, *stn1*-Δ, and *ten1*-Δ null strains are inviable, several prior observations have suggested that the lethality of strains bearing null mutations in this complex might be partially bypassed by loss of *RAD24* function (Weinert *et al.* 1994; Lydall and Weinert 1995; Small *et al.* 2008). We examined this by monitoring growth of *cdc13*-Δ and *cdc13*-Δ *rad24*-Δ isolates following dissection of a *cdc13*-Δ/*CDC13 rad24*-Δ/*RAD24* diploid strain. Whereas 22 *cdc13*-Δ strains were capable of only one to two cell divisions, all 22 *cdc13*-Δ *rad24*-Δ newly generated haploid strains underwent sufficient cell divisions to form a microcolony (a representative example is shown in Figure 3A). This behavior extended to the other subunits of the proposed t-RPA complex: 30 of 30 *stn1*-Δ strains and 22 of 22 *ten1*-Δ strains arrested after one to two cell divisions, whereas 29 of 30 *stn1*-Δ *rad24*-Δ strains and 21 of 22 *ten1*-Δ *rad24*-Δ strains produced microcolonies. These *cdc13*-Δ *rad24*-Δ, *stn1*-Δ *rad24*-Δ, and *ten1*-Δ *rad24*-Δ microcolonies were not capable of further propagation, although rare "escaper" clones could be recovered at very low frequencies (data not shown). Figure 3A further demonstrates that the ability to partially bypass *cdc13*-Δ lethality was a property that extended to other members of the *RAD24* epistasis group (Lydall and Weinert 1995; Paulovich *et al.* 1997), as *cdc13*-Δ *rad17*-Δ and *cdc13*-Δ *mec3*-Δ strains exhibited a comparable ability to form microcolonies.

The ability to observe a limited degree of growth in t-RPA null strains in the absence of *RAD24* function provided an assay for examining whether this phenotype was also sensitive to temperature. To test this, the *cdc13*-Δ/*CDC13 rad24*-Δ/*RAD24* diploid strain was dissected at 23°, 26°, 28°, 30°, 32°, 34°, and 36°, and *cdc13*-Δ *rad24*-Δ spore products were identified. Microcolony size demonstrated a reduction in size (more than twofold) for microcolonies grown at 34° and 36° *vs.* at lower temperatures (Figure 3, B and C). Similar results were observed when comparing multiple *stn1*-Δ *rad24*-Δ

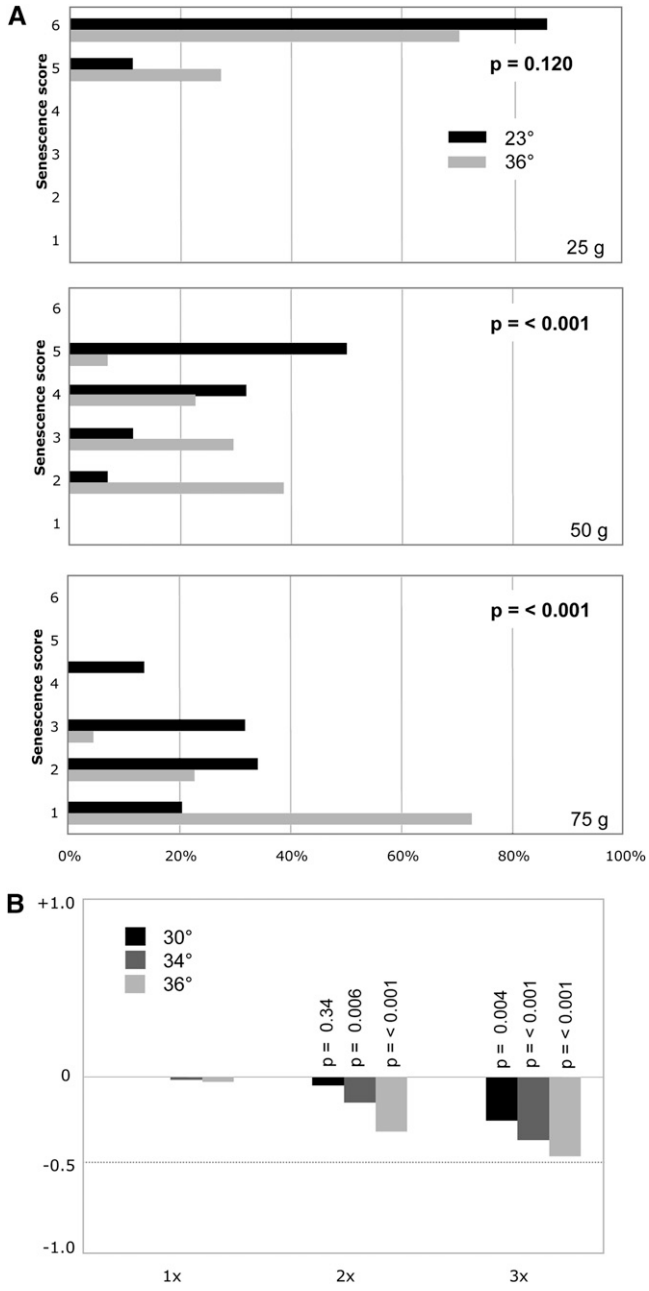

Figure 2 (A) Histogram displaying the growth characteristics of 42 *tlc1*-Δ isolates grown at 23° *vs.* 36° for three successive streak-outs, corresponding to ~25, ~50, and ~75 generations of growth; isolates were scored for six phenotypic categories, ranging from a scale of 1 (severe senescence) to 6 (comparable to wild-type growth), and a Student's *t*-test was used to assess the statistical significance between the two temperatures, as described previously (Gao *et al.* 2010). (B) Averaged phenotypic scores for the 42 *tlc1*-Δ isolates propagated at 30°, 34°, or 36° were normalized to growth at 23°, with a negative value indicating enhanced senescence at a given time point, relative to the behavior of the same set of isolates at 23°.

isolates following dissection of a *stn1*-Δ/*STN1 rad24*-Δ/*RAD24* diploid strain at 23°–36° (Figure 3D). Thus, similar to the situation with telomerase-defective yeast strains, the consequence of loss of the t-RPA complex is sensitive to elevated temperatures.

Analysis of current temperature-sensitive alleles of CDC13 and STN1

Since even strains with null mutations in *CDC13* and *STN1* are susceptible to growth temperature, this prompted us to re-examine the characteristics of previously isolated ts mutations in these genes. In particular, we asked whether strains with previously described ts alleles displayed the properties expected for a *bona fide* temperature-sensitive mutation: fully functional at permissive temperature(s) *vs.* null (or greatly reduced for function) at nonpermissive temperature(s).

The widely used *cdc13-1* strain exhibits reduced viability at 23° and lethality at 25°–26°. Growth is further impaired by the presence of mutations in other telomere-related genes; for example, *cdc13-1 tlc1*-Δ and *cdc13-1 yku80*-Δ strains are extremely sick at 23° (Nugent *et al.* 1996; Polotnianka *et al.* 1998). The severity of this synthetic phenotype suggested that Cdc13 function was impaired even at permissive temperatures. In fact, examination of steady-state protein levels of the mutant Cdc13-1-$(myc)_{18}$ protein compared to the wild-type Cdc13-$(myc)_{18}$ protein (expressed on a *CEN* plasmid in a wild-type protease-deficient strain) did not reveal behavior consistent with a thermolabile protein. Instead, the Cdc13-1-$(myc)_{18}$ mutant protein displayed a fourfold reduction in protein levels at 23°, relative to the wild-type protein, and Cdc13-1-$(myc)_{18}$ levels were not reduced further when the strain was incubated at 36° (Figure 4A). These observations argue that the *cdc13-1* mutation results in a hypomorphic protein that is associated with a substantial reduction in protein levels (and presumably function) even at permissive temperatures, thereby explaining the synthetic growth characteristics. The Cdc13-1 protein may be thermosensitive as well, but the lack of change in protein levels at 36° *vs.* 23° suggests that at least some Cdc13 function is retained at higher temperatures. Consistent with this, *in vivo* association of the mutant Cdc13-1 protein with telomeres is unchanged at 37° relative to 23° (Vodenicharov and Wellinger 2006), arguing that the Cdc13-1 protein still retains DNA-binding activity and potentially other functions at 36°. We propose that the phenotypes exhibited by a *cdc13-1* strain are due to a severe hypomorphic mutation in *CDC13* combined with the Tmp^- phenotype, rather than due to conditional depletion of the Cdc13 protein.

For *STN1*, two mutations, *stn1-13* and *stn1-63*, have been used in several previous studies (Grandin *et al.* 1997; Puglisi *et al.* 2008). The *stn1-13* allele (containing six missense mutations throughout the protein) is only minimally impaired for growth even at 37° (Grandin *et al.* 1997, 2001; data not shown), and thus it was not included in our subsequent analysis. The *stn1-63* strain (Puglisi *et al.* 2008), which contains a single missense mutation in the essential N-terminal domain (D99E), showed a more substantial impairment for growth at 36° although the strain was not completely inviable at this temperature (Figure 4B). Somewhat surprisingly, FACS analysis revealed that the *stn1-63* strain did not exhibit a pronounced defect in cell-cycle

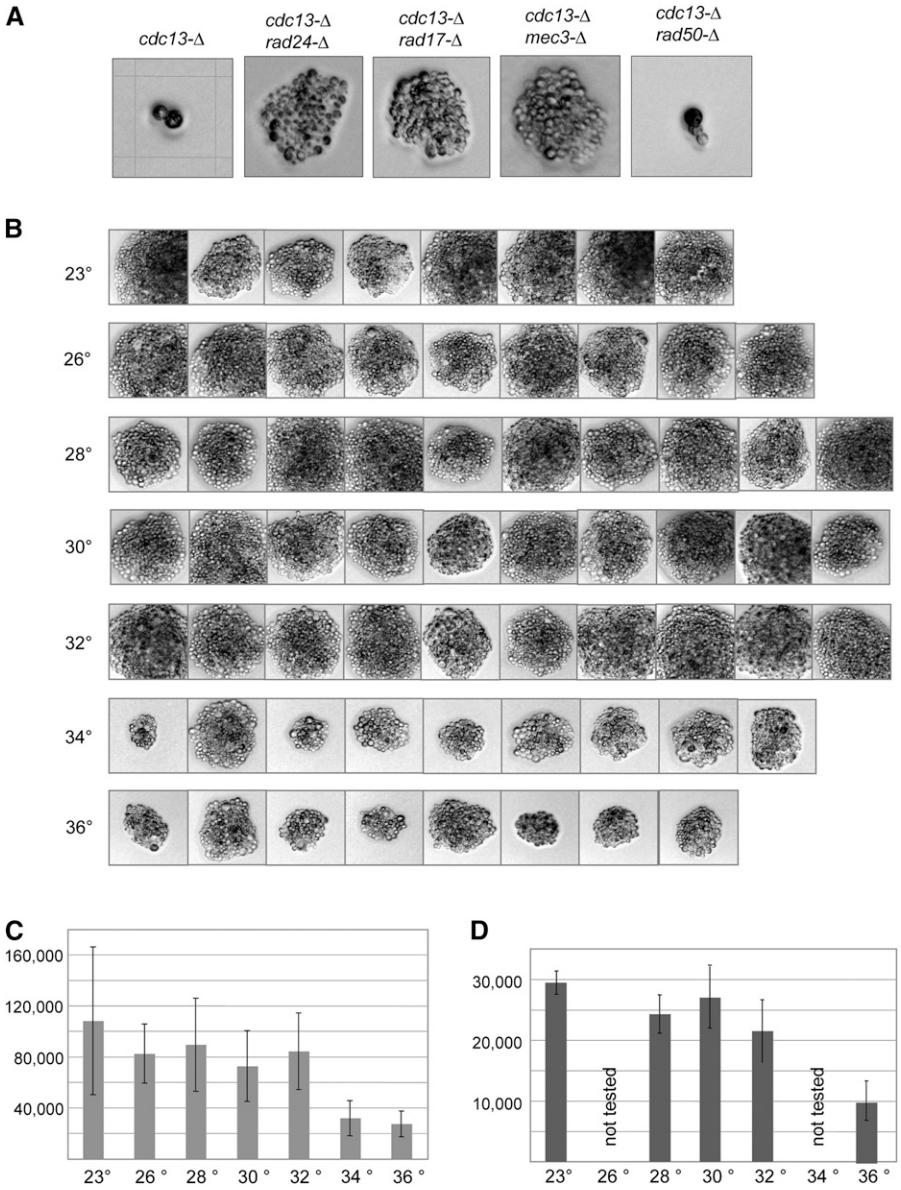

Figure 3 Microcolony growth of *cdc13*-Δ *rad24*-Δ and *stn1*-Δ *rad24*-Δ strains is temperature-sensitive. (A) Isogenic diploid strains bearing null mutations of the indicated genotype were dissected, and germinated spores were photographed after growth was complete (48 hr at 30°, 32°, 34°, and 36° or 72 hr at 23°, 26°, and 28°) with a Zeiss Axioskop 50 with a Nikon Digital Sight DS-5M camera; multiple isolates were examined for each genotype, and representative examples are shown. The grid on the *cdc13*-Δ image corresponds to 62.5 × 62.5 μm; all images were at the same magnification. (B) Photographs of *cdc13*-Δ *rad24*-Δ microcolonies from germinated spores generated by dissection of the *cdc13*-Δ/*CDC13 rad24*-Δ/*RAD24* strain, following incubation for 3 days at the indicated temperature. (C) Each *cdc13*-Δ *rad24*-Δ microcolony image shown in B was selected, and the sum of the pixels in the selected area was quantitated using Photoshop. The maximum and minimum values were eliminated from each temperature group; mean and standard variation are shown. (D) Quantitation of *stn1*-Δ *rad24*-Δ microcolonies from a *stn1*-Δ/*STN1 rad24*-Δ/*RAD24* strain, processed as described in B and C. The *stn1*-Δ *rad24*-Δ microcolonies were approximately two- to threefold smaller than *cdc13*-Δ *rad24*-Δ microcolonies, although the experiments shown in C and D were performed separately, which precluded a more quantitative comparison.

progression at 36° (Figure 4B), as would be expected if a subunit of the t-RPA complex had been depleted by a conditional lethal mutation. A more careful examination of the growth of the *stn1-63* strain revealed that a reduction in viability was observed only at 34° and 36° (Figure 4C). Steady-state protein levels of the Stn1-63-$(myc)_7$ mutant protein were also unaffected when the culture was shifted to higher temperature (Figure 4D), in contrast to the expectations for a thermolabile protein that should be depleted (or at least diminished) at the nonpermissive temperature. Furthermore, as previously observed (Puglisi *et al.* 2008), the *stn1-63* strain exhibited greatly elongated telomeres even at 23° (Figure 4E), indicating that the Stn1 protein is substantially impaired even at permissive temperature. These data indicate that the *stn1-63* mutation, like *cdc13-1*, encodes a hypomorphic protein that exhibits a temperature-independent defect, rather than a thermolabile mutant protein. We hypothesize that the reduced growth at 34°–36° in the *stn1-63* strain background is also an additive effect, due to a partial loss-of-function defect in *STN1* in combination with the Tmp^- phenotype. This hypothesis is tested further in a later section that examines an expanded panel of missense mutations in *STN1*.

Since protein levels and/or function appeared to be severely impaired at the presumed permissive temperature for the existing *cdc13* and *stn1* alleles, we conclude that these alleles are not *bona fide* conditional lethal reagents. This prompted us to screen for new ts alleles of *CDC13* and *STN1*, as described in the following sections, with the goal of identifying alleles in each gene that are fully functional under permissive conditions (such as 23°) and completely null for function under nonpermissive conditions (such as ≤32°) that would be minimally influenced by the Tmp^- phenotype.

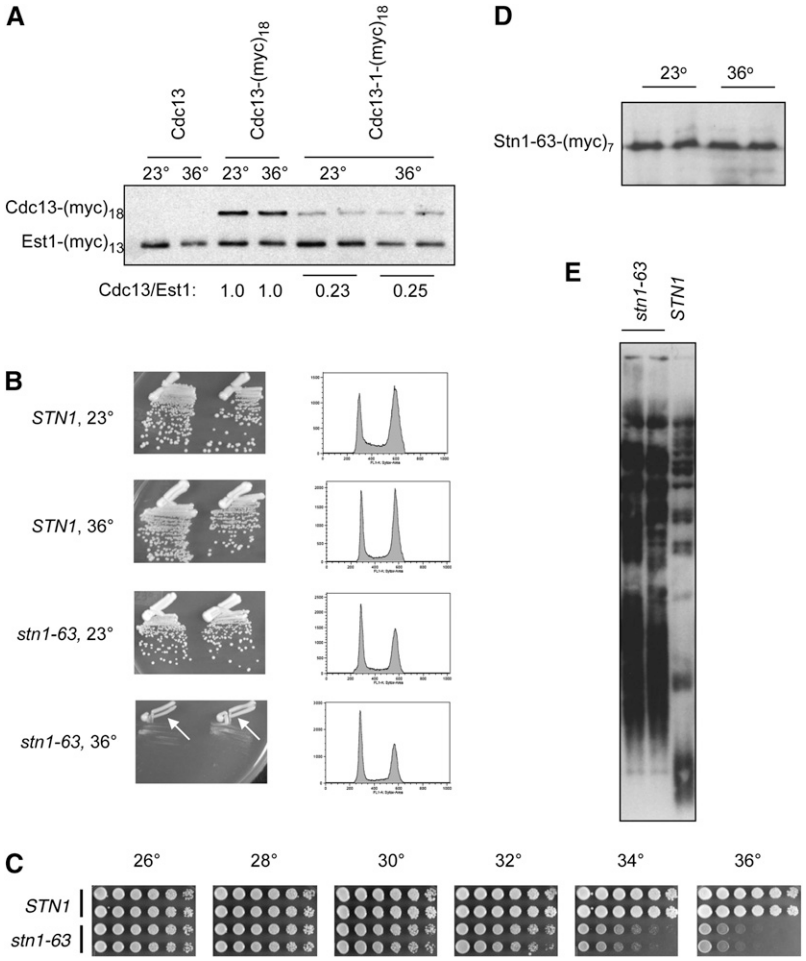

Figure 4 The *cdc13-1* and *stn1-63* mutations behave like hypomorphic alleles. (A) Steady-state protein levels of the wild-type Cdc13-(myc)$_{18}$ and mutant Cdc13-1-(myc)$_{18}$ proteins, expressed from a *CEN* vector; extracts were prepared from strains grown at 23° or at 36° for 3.5 hr and analyzed by anti-*myc* Western analysis on 8% SDS-PAGE. The strain also expresses an Est1-(myc)$_{13}$ protein (as an integrated tagged construct), which provided an internal control for protein levels. (B) Comparison of *stn1-Δ*/p*CEN STN1 vs. stn1-Δ*/p*CEN stn1-63*, as assessed by single-colony propagation on rich media (Left panels) or cell-cycle progression of liquid cultures (Right panels) grown at 23° and 36°; arrows indicate that cell division still occurs at 36°. (C) Viability of *RAD24* and *rad24-Δ* versions of the *stn1-Δ*/p*CEN stn1-63* strain at the indicated temperatures; serial dilutions were plated on prewarmed rich media plates and photographed after 2.5 days (for ≥28° incubations) or after 4 days (for 23° and 25° incubations). (D) Steady-state protein levels of the Stn1-63-(myc)$_7$ protein, expressed from a *CEN* vector, assessed as described in A. (E) Telomere length of the *stn1-Δ*/p*CEN stn1-63* strain compared to the isogenic *stn1-Δ*/p*CEN STN1* strain at 23°.

Identification of new temperature-sensitive alleles of CDC13 using both forward and reverse mutagenesis

Two forward mutagenesis screens were performed, mutagenizing either the full-length *CDC13* gene by passage through an *E. coli* mutator strain or the essential DBD of *CDC13* (Mitton-Fry *et al.* 2002) by low-fidelity PCR. Both collections of mutagenized plasmids were transformed into a *cdc13-Δ* shuffle strain kept alive by the presence of a covering *CEN URA3 CDC13* plasmid, and yeast transformants were screened for ts growth by replica-plating onto media that selected for loss of the covering plasmid (see *Materials and Methods* for details). Rescued plasmids were subsequently retested following retransformation into the *cdc13-Δ* shuffle strain and sequenced to identify mutation(s).

Screening the mutagenized full-length *CDC13* gene resulted in 26 candidate *cdc13-ts* alleles, corresponding to 7 unique mutations (Supporting Information, Figure S1). Five alleles contained a single missense mutation: 1 mutation in the N terminus of the protein (*cdc13-S56F*), 3 mutations in the DBD (*cdc13-V530G*, *cdc13-S531F*, and *cdc13-D546G*) and 1 C-terminal allele (*cdc13-T847M*). The remaining 21 alleles had a frameshift mutation at either residue 686 (2 isolates) or residue 707 (19 isolates), resulting in truncation of the protein just past the boundary of the DBD (with either 10 or 65 amino acids added to the end of the protein as a result of the frameshift mutation). Recovery of these two frameshift mutations, as well as of *cdc13-T847M*, was somewhat unexpected because a previously well-characterized allele of *CDC13* (*cdc13-5*), which contained a stop codon introduced at amino acid 694, does not exhibit thermolabile growth (Chandra *et al.* 2001 and Figure S2).

The second screen, which targeted the DBD of *CDC13*, yielded 18 alleles with ts phenotypes. Sequence analysis revealed that all but two of these alleles had multiple missense mutations, a common problem with error-prone PCR protocols. However, several clusters of amino acids (aa 525–544, 611–618, and 683–684) appeared to be overrepresented (Figure S2), suggesting that this information might be useful in identifying the causative mutation for at least a subset of these 18 isolates. Therefore, a panel of single missense mutations in residues in these clusters was constructed and tested for ts growth. This analysis identified 6 alleles—*cdc13-L529Q*, *cdc13-V543F*, *cdc13-S611L*, *cdc13-G614V*, *cdc13-F683L*, and *cdc13-F684S*—which conferred a ts phenotype with impaired growth at temperatures ranging from 30° to 36° (Figure S1).

In parallel with these two forward mutagenesis screens, we also employed reverse mutagenesis, using a computational

method called Evolutionary Trace (ET) to identify residues in the DBD domain as targets for reverse mutagenesis. ET combines structural information with amino acid diversity to determine the evolutionary pressure at a given residue, which can identify functionally significant residues (Lichtarge *et al.* 1996; Lichtarge and Sowa 2002). A total of 14 amino acids in Cdc13 with an ET score of ≤10% were selected for mutagenesis (excluded from this set were residues that contact DNA, which are under analysis in a separate study in this laboratory). Each residue was mutated to alanine, and the resulting collection of plasmids were introduced into a *cdc13-Δ* shuffle strain and assayed as described above. Four of these 14 strains displayed growth defects: one allele, *cdc13-D546A*, conferred lethality (data not shown), whereas strains expressing alanine mutations in three residues (F547, N609, and F684) exhibited ts growth (Figure S1).

Collectively, these three screens yielded missense mutations in 13 amino acids of Cdc13 that conferred conditional lethal growth. To determine which of these *cdc13-ts* alleles were fully functional at permissive temperatures but null with regard to both phenotype and protein levels at higher temperatures, we initially examined cell-cycle progression at 23° and 36°. Two mutants (*cdc13-V543F* and *cdc13-T847M*) did not exhibit a complete cell-cycle arrest at 36°, and one mutant (*cdc13-S56F*) had a slight cell-cycle delay even at 23° (data not shown); these three mutants were discarded from further analysis. As a next step, seven mutants that were fully viable at temperatures >28° were examined for Cdc13 protein levels (mutant strains with defects in viability at ≤28° were not analyzed, on the assumption that this would correlate with reduced function and/or protein levels even at permissive temperatures). Each of these seven mutations were introduced into a plasmid construct expressing Cdc13-$(myc)_{18}$, and extracts prepared from strains expressing these mutant Cdc13-$(myc)_{18}$ proteins grown at 23° and 36° were examined for protein levels by Western analysis. In contrast to the Cdc13-1 protein (Figure 4A), all seven mutant proteins behaved like thermolabile proteins, with protein levels substantially reduced at 36°, relative to protein levels at 23° (Figure 5A). However, two mutant proteins displayed greater than threefold reduction in protein levels even at 23° (*cdc13-F547A* and *cdc13-L529A*) and were excluded from the next stage of analysis.

Each of the remaining five mutations were integrated into the genome in place of the wild-type *CDC13* gene for subsequent analysis to exclude possible artifacts due to variations in plasmid copy number and/or altered gene expression by plasmid-borne alleles. The resulting *cdc13-ts* strains were screened for effects on viability and cell-cycle progression at a range of temperatures between 23° and 34°. Cell viability assays demonstrated that these new *cdc13-ts* alleles were fully viable at 28° and inviable at temperatures ranging from 30° to 33° (Figure 5B). It is also worth noting that each of the resulting integrated strains exhibited a ts phenotype that was slightly more severe than the comparable mutation when examined on a *CEN* plasmid in a *cdc13-Δ* null strain

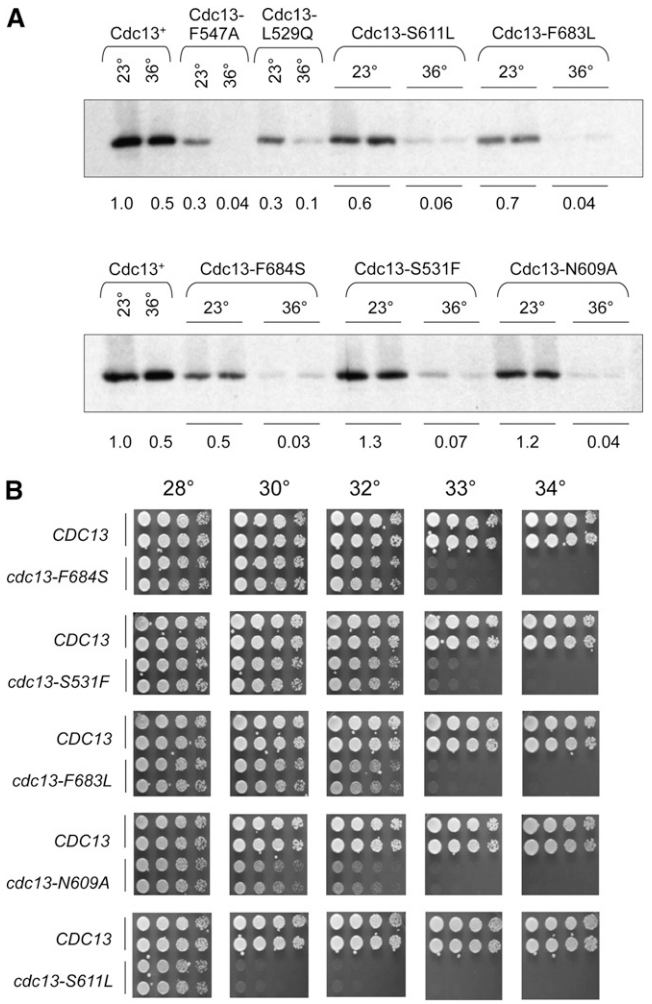

Figure 5 Characterization of new *cdc13-ts* mutations. (A) Steady-state protein levels of mutant Cdc13-$(myc)_{18}$ proteins compared to wild-type Cdc13-$(myc)_{18}$, assessed as in Figure 4A. (B) Viability of the indicated strains, with *cdc13-ts* mutations integrated into the genome, assessed as in Figure 4C.

(compare Figure S1 with Figure 5B). This parallels previous comparisons from our laboratory of the viability of the *cdc13-1* allele as an integrated *vs.* plasmid-borne allele (data not shown), as well as comparisons of integrated *vs.* plasmid-borne *stn1⁻* and *ten1⁻* alleles (Paschini *et al.* 2010).

A return-to-viability experiment demonstrates that phenotypes of cdc13-ts strains at 34°–36° are not solely due to loss of CDC13 function

These *cdc13-ts* mutant strains provide a set of reagents for analysis of *CDC13* under conditions where Cdc13 is functional at 23° and fully impaired at temperatures <34°–36°. As a first step in assessing this, we repeated a return-to-viability experiment that has previously been used to analyze Cdc13-related defects in the presence or absence of *RAD9* function in a *cdc13-1* strain (Weinert and Hartwell 1993; Lydall and Weinert 1995; Addinall *et al.* 2011). In this protocol, *cdc13-1* cells grown at 23° are shifted to

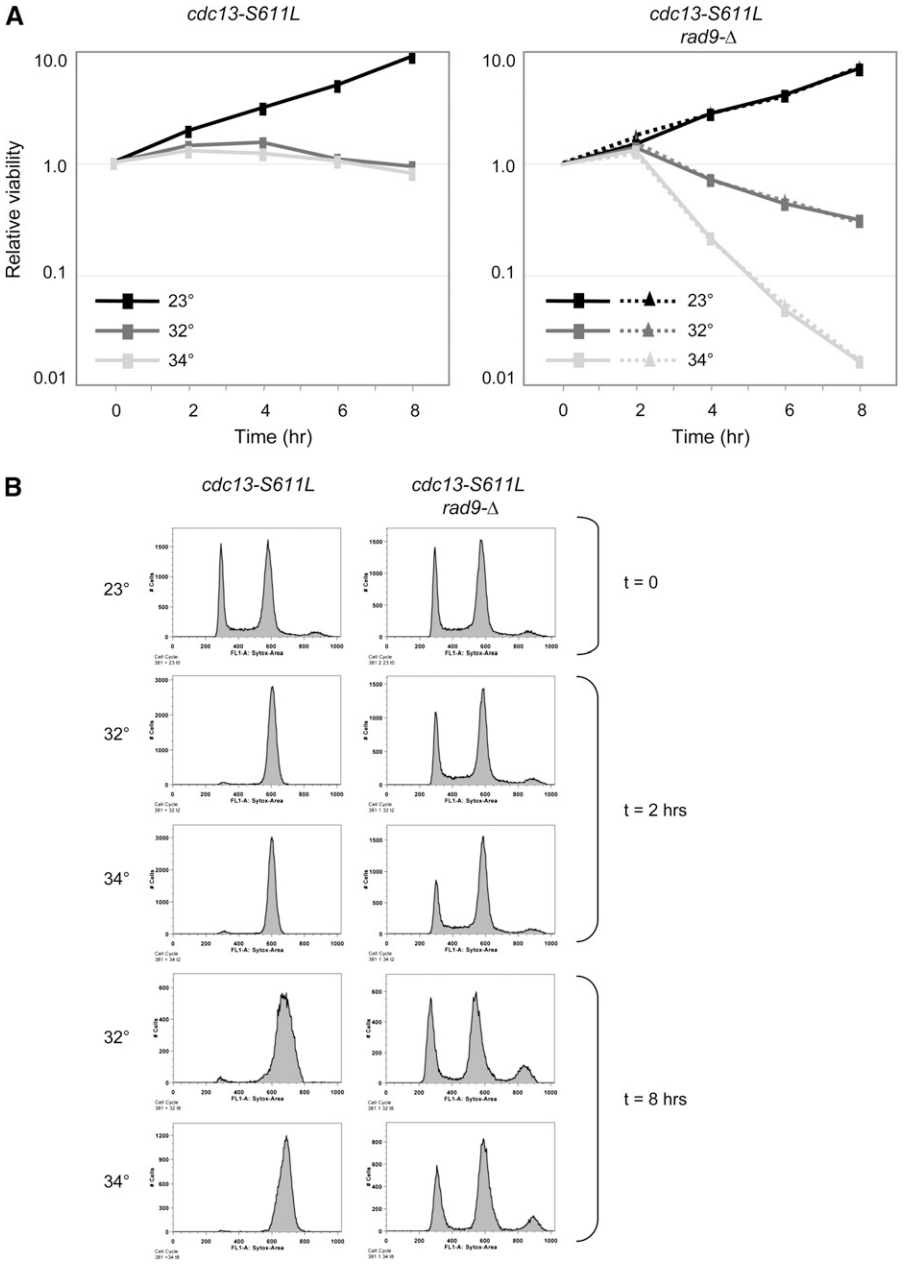

Figure 6 Temperature-dependent effects on viability of a *cdc13-S611L rad9*-Δ strain. (A) Mid-log cultures of *cdc13-S611L* (Left) or *cdc13-S611L rad9*-Δ (Right, duplicate samples) strains grown at 23° were shifted to the indicated temperatures and incubated for up to 8 hr; viability was determined by plating appropriate dilutions on rich media plates that were incubated at 23° for 3 days. Three independent repetitions of this experiment produced essentially identical results. (B) Flow cytometry profile of log-phase cultures of the indicated strains from the experiment shown in A, fixed and stained with SYTOX green.

nonpermissive temperature for varying time periods and subsequently assessed for viability at permissive temperature (23°). Prior versions of this experiment have used 36° or 38° as the nonpermissive temperature, whereas in the experiment presented here, the *cdc13-S611L* strain was incubated at 32°, 34°, or 36°. As expected on the basis of the observations in Figure 5B, *cdc13-S611L* cells failed to undergo cell division when incubated for 8 hr at 32°, which was accompanied by a cell-cycle arrest. The response at 32° was indistinguishable from that at 34° (Figure 6, A and B), confirming that 32° was fully nonpermissive for this *cdc13-ts* strain.

Consistent with previous analysis of the *cdc13-1* strain (Weinert and Hartwell 1993), arrest of the *cdc13-S611L* strain resulted in no more than a 1.5-fold loss of viability, even after 8 hr at 32°, 34°, or 36° (Figure 6A and data not shown). As was also expected from prior observations, loss of *RAD9* function prevented cell-cycle arrest when the *cdc13-S611L rad9*-Δ strain was incubated at 32° (Figure 6B). Incubation of *cdc13-S611L rad9*-Δ cells at the nonpermissive temperature (32°) was accompanied by a modest reduction in viability (5-fold by 8 hr). However, when cells were incubated at 34°, there was a striking effect in the absence of *RAD9* function, as viability was reduced 65-fold at the 8-hr time point (Figure 6A). Increasing the incubation temperature to 36° reduced viability even further (data not shown). Thus, the *RAD9*-dependent effect at 34°–36°, which was well above the nonpermissive temperature for the *cdc13-S611L* strain, indicated that an additional defect that is independent of *CDC13* function, but *RAD9*-dependent, contributed to inviability at 34°–36°.

Reverse mutagenesis of the essential N-terminal domain of STN1

In an attempt to recover conditional lethal alleles of *STN1*, we employed two reverse mutagenesis strategies that targeted the essential N-terminal domain of the protein. Because the ET protocol was so effective with *CDC13* (3 of 14 mutations yielded a thermolabile protein, including 2 of the mutations shown in Figure 5), ET was similarly applied to the predicted OB-fold domain of *Stn1*. The top 20 residues were mutated to alanine, and a subset were also mutated to serine. These 30 *stn1* missense mutations were transformed into a *stn1*-Δ/p *CEN URA3 STN1* strain, and yeast transformants were screened for ts growth following loss of the covering plasmid (Figure S3 and data not shown). Roughly half of these mutant strains had no notable growth defect and were eliminated from further analysis. The remaining strains exhibited a range of growth phenotypes, which fell into roughly three categories. One subset (*stn1-N67A*, *stn1-E167A*, *stn1-W171S*, *stn1-L181S* *stn1-L70A*, *stn1-I73S*, and *stn1-G77A*) grew approximately as well as wild type at lower temperatures but exhibited growth defects at 34°–36° (Figure S3); however, examination of telomere length revealed that substantial telomere elongation had occurred even when these strains were grown at permissive temperature (Figure S4 and data not shown). Strains in the second category (*stn1-L41S*, *stn1-F64A*, *stn1-F64S*, and *stn1-L70S*) were somewhat impaired for growth at temperatures ranging from 23° to 34°, with the growth phenotype more severe at 36°; all four of these strains exhibited even more extensive telomere elongation at 23° (Figure S3 and Figure S4). The last category (*stn1-G77S*, *stn1-D98A*, and *stn1-D99A*) exhibited the most severe growth defect, as all three strains were barely viable at temperatures up to 32°–34° and inviable at 36° (Figure S3). In every case, the growth defect associated with a given mutation became more pronounced at 36°, a pattern that was very similar to that described above in Figure 4 for *stn1-63*. Furthermore, cell-cycle progression as assessed by FACS demonstrated that the reduced growth at high temperatures did not exacerbate the relatively modest cell-cycle defect displayed by most of these mutants (Figure S3 and data not shown). Thus, this first attempt at recovering one or more ts alleles of *STN1* appeared to be unsuccessful.

However, inspection of the position of this collection of mutations on the predicted structure of the Stn1 protein suggested a possible structural correlation: mutations with the most severe growth defects were located in residues that comprised, or were in close proximity to, the β-barrel of the OB-fold (G77, L70, D98, D99). This suggested that mutagenesis that targeted this particular region of the Stn1 protein might be more successful. Specifically, we directed our attention to a panel of 11 hydrophobic residues (I73, L75, I79, I93, L97, L106, L140, V142, L153, V155, and L158) with side chains located in the interior of the β-barrel of Stn1, on the assumption that (partial) destabilization of the OB-fold might have a higher probability of generating thermosensitive proteins. Each of these 11 residues were mutated to alanine, serine, and tyrosine (based on the results described above for Cdc13, which indicated that restricting mutagenesis to alanine missense mutations might be insufficient). The resulting panel of 33 plasmids bearing *stn1* missense mutations in the β-barrel were introduced into a *stn1*-Δ shuffle strain and examined at a range of temperatures from 23° to 36°. Not unexpectedly, a large number (27%) of the resulting strains were inviable or nearly inviable. Many of the viable strains exhibited a range of growth defects and, once again, the severity of the defect was enhanced in each case when the strains were propagated at 34°–36° (summarized in Figure S5). Furthermore, the majority of the viable strains exhibited elongated telomeres even when the strains were propagated at permissive temperatures (Figure S4). Only two residues, L106 and L140, appeared to be immune to mutagenesis, as the strains expressing mutations in either amino acid exhibited wild-type growth at all temperatures with no telomere length defect, despite the fact that these two bulky hydrophobic residues were predicted to be on the interior of the barrel of the OB-fold (data not shown).

Analysis of integrated stn1⁻ alleles

Very few, if any, of the panel of *stn1⁻* mutations described above behaved as expected for a thermolabile protein. However, in a previous study, we observed differences in viability when comparing *stn1⁻* alleles present on a plasmid in a *stn1*-Δ strain *vs.* integrated into the genome (Paschini *et al.* 2010). Since this current set of *stn1⁻* mutations was also expressed on a *CEN* plasmid in a *stn1*-Δ strain, we considered the possibility that fluctuations in plasmid copy number might mask a ts phenotype. To test this, diploid strains that were heterozygous for *STN1* were constructed by integrating candidate *stn1-ts* alleles into the genome (see *Materials and Methods* for details), and haploid *stn1* strains were generated by dissection. Five alleles (*stn1-I73A*, *stn1-I73S*, *stn1-I79S*, *stn1-G137A*, and *stn1-G137S*) were chosen for this analysis on the basis of the magnitude of the difference comparing growth at 23° *vs.* 36° when assessing the plasmid-based phenotype in a *stn1*-Δ strain (Figure S3 and Figure S5).

Dissection of the *stn1-I73S*/*STN1* diploid revealed that the haploid *stn1-I73S* strain was inviable, as germinated *stn1-I73S* spores were capable of undergoing only one to two divisions even at 23° (Figure 7A). This indicates that *stn1-I73S* is a null mutation, since *stn1-I73S* and *stn1*-Δ strains resulted in the same phenotype following dissection. Furthermore, germinated *stn1-I73S* *rad24*-Δ spores were capable of forming microcolonies (Figure 7A), similar to our observations for *stn1*-Δ *rad24*-Δ. Therefore, the apparent ts plasmid-based phenotype (viable at 23°–32° and inviable at ≥34°) was not due to a thermolabile protein; consistent with this, Western analysis did not reveal any change in steady-state levels of the Stn1-I73S protein when examined

by Western analysis from extracts grown at 23° *vs.* 36° (data not shown). We postulate that viability of the *stn1*-Δ strain expressing the plasmid-borne *stn1-I73S* mutation was due to increased plasmid copy number in response to selective pressure for viability.

In contrast, dissection of the other heterozygous strains gave rise to viable *stn1*$^-$ haploid strains. Among this set of four strains, only the *stn1-I73A* strain exhibited a possible thermosensitive phenotype, as the mutant strain exhibited a notable growth defect at 30° compared to 23°, although growth was once again more severely affected at 34°–36° (Figure 7B). This slow gradient of impairment suggested that the *stn1-I73A* mutation might encode a partially defective protein even at permissive temperatures. Consistent with this, telomere length was substantially affected in the *stn1-I73A* strain even at 23°, although telomeres were further elongated when the strain was propagated at higher temperatures (Figure 7C). Thus, we conclude that *stn1-I73A* encodes a protein that is most likely both hypomorphic and thermolabile, with a partial loss of function at permissive temperature that is further exacerbated by growth at higher temperatures.

Re-examination of a cdc13-1 suppressor reveals a complex genetic interaction between null mutations, cold sensitivity, and the Tmp$^-$ *phenotype*

Several genome-wide screens for genes that enhance or suppress the ts growth of a *cdc13-1* strain have yielded several hundred genes, implicating a wide number of molecular pathways in telomere capping (Downey *et al.* 2006; Addinall *et al.* 2008). The analysis above indicates that temperature alone can impact telomere-related phenotypes, which adds an additional layer of complexity when interpreting the results from *cdc13-1*-based screens. To investigate this more closely, we re-examined one candidate (*CGI121*) recovered from a *cdc13-1* suppressor screen. Since loss of Cgi121 function is capable of rescuing the temperature-dependent growth defects displayed by the hypomorphic *cdc13-1* strain and a *yku80*-Δ null strain (Downey *et al.* 2006), we asked whether a *cgi121*-Δ mutation would have a similar impact on the senescence phenotype of a *tlc1*-Δ strain or on the microcolony growth of a *cdc13*-Δ *rad24*-Δ strain.

Dissection of *cgi121*-Δ/*CGI121* diploids revealed an unexpected surprise, however: the *cgi121*-Δ strain was itself cold-sensitive for growth. A comparison of colony sizes for *CGI121 vs. cgi121*-Δ strains following sporulation at 23°, 30°, and 36° demonstrated that the *cgi121*-Δ strain exhibited a substantial growth defect at 23°, which was largely alleviated by growth at 36° (Figure 8A). A re-examination of previously published data by Durocher and colleagues indicates that a cold-sensitive growth defect had been previously observed for *cgi121*-Δ as well as for a strain with a null mutation in *BUD32* (another member of the same complex) (Downey *et al.* 2006), supporting the results reported here. Thus, the growth phenotype of a *cgi121*-Δ strain is the consequence of two activities: loss of Cgi121 function combined with an activity that is naturally impaired for function at 23° but not at 36°.

To assess for effects on senescence, *tlc1*-Δ and *tlc1*-Δ *cgi121*-Δ strains were propagated for ~75 generations following dissection at either 32° or 36° (at lower temperatures, the significant growth defect due to *cgi121*-Δ overwhelmed the senescence phenotype). As shown in Figure 8B, loss of Cgi121 function significantly attenuated senescence at both temperatures. Thus, a null mutation in *CGI121* acts as a partial bypass suppressor of a null mutation in telomerase, at least at high temperatures. In contrast, the genetic interaction between null mutations in *CGI121* and *CDC13* was more complex. At 23°, the *cgi121*-Δ mutation was capable of bypassing the near-lethality of a *cdc13*-Δ *rad24*-Δ strain: *CDC13* was no longer an essential gene in a *cgi121*-Δ *rad24*-Δ background, such that *CDC13 cgi121*-Δ *rad24*-Δ and *cdc13*-Δ *cgi121*-Δ *rad24*-Δ strains gave rise to equally sized (although small) colonies (Figure 8C). However, at higher temperatures, the difference between these two sets of strains became more obvious (Figure S6). This reveals a complex genetic interaction between the cold-sensitive growth properties of the suppressor strain (*cgi1121*-Δ) and the temperature-enhanced phenotypes of the *cdc13*-Δ *rad24*-Δ strain, as four genetic factors contributed to the growth characteristics of the *cdc13*-Δ *cgi121*-Δ *rad24*-Δ strain at different temperatures (loss of Cdc13 function, loss of Cgi121 function, the Tmp$^-$ phenotype, and the cold-sensitive activity). Thus, whether the enhanced growth properties of the *cdc13*-Δ *cgi121*-Δ *rad24*-Δ strain are due to a genetic relationship between *CDC13* and *CGI121* cannot be determined.

Discussion

The results presented here, as well as in several prior studies, establish that there is an additional phenotypic consequence at telomeres when cells are grown at higher temperatures, particularly >34°. This phenotype can be observed even in wild-type yeast and also contributes to the severity of phenotypes displayed by yeast strains bearing null mutations in the Ku heterodimer (Feldmann and Winnacker 1993; Boulton and Jackson 1996; Feldmann *et al.* 1996), telomerase (Figure 2), and the t-RPA complex (Figure 3). We propose that the enhanced phenotype at higher temperatures is a synthetic genetic effect, as illustrated schematically in Figure 9, due to a mutation in a telomere-related complex combined with an additional defect that becomes particularly apparent at 34°–36°.

This temperature-dependent defect also complicates the analysis of missense mutations in subunits of each of these complexes, particularly for the essential genes *CDC13*, *STN1*, and *TEN1*, which suggests that a number of mutations in these three genes have been incorrectly categorized as temperature-sensitive alleles and are instead hypomorphic alleles. In particular, several observations argue against the long-standing assumption that *cdc13-1* encodes a conditional

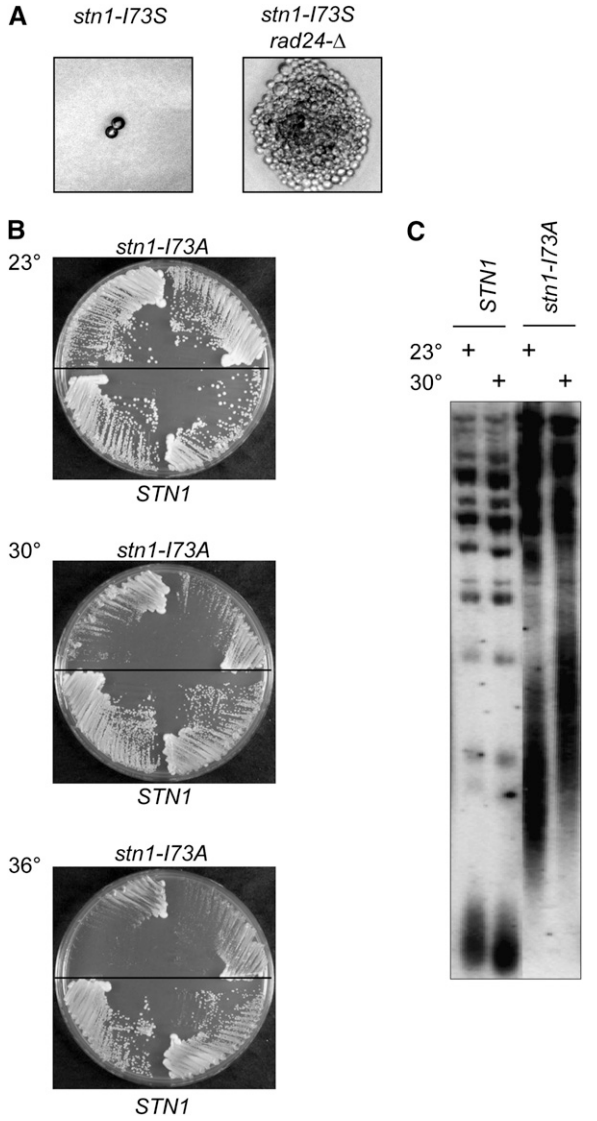

Figure 7 Characterization of *stn1-I73S* and *stn1-I73A* strains. (A) Photomicrographs of germinated *stn1-I73S* and *stn1-I73S rad24-*Δ spores. (B) Single-colony streak-outs of isogenic *stn1-I73A* and *STN1* haploid strains (generated by dissection of a *stn1-I73A/STN1* diploid) incubated at 23°, 30°, and 36°. (C) Telomere-length analysis of *stn1-I73A* and *STN1* isolates from B after ~40 generations of growth at 23° or 30°.

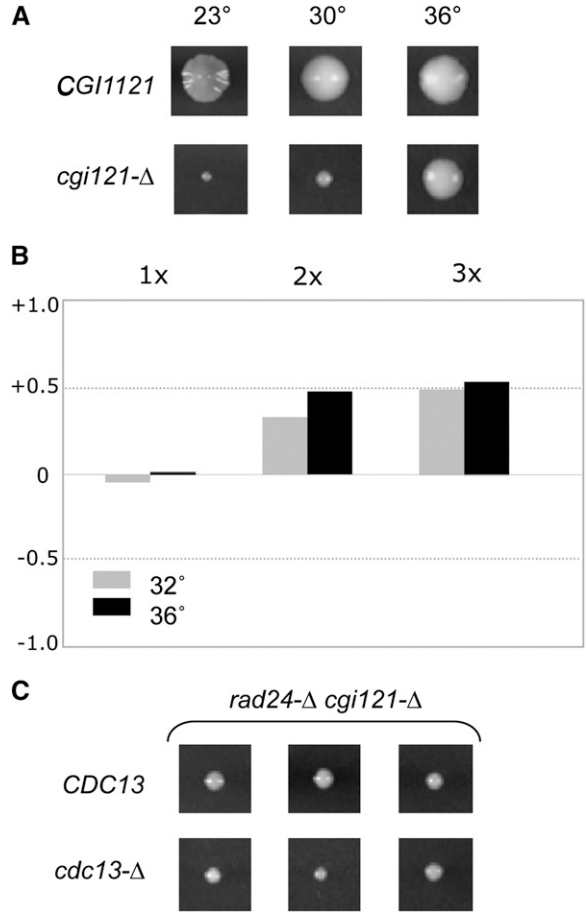

Figure 8 Loss of *CGI121* function bypasses null mutations in *CDC13* and telomerase. (A) Comparison of colony sizes of *CGI121* and *cgi121-*Δ isogenic strains propagated at the indicated temperatures. (B) Comparison of the senescence phenotypes of 26 *tlc1-*Δ *CGI121* isolates with 22 *tlc1-*Δ *cgi121-*Δ isolates at 32° and 36°, analyzed as in Figure 2B. (C) Three colonies each of *cdc13-*Δ *cgi121-*Δ *rad24-*Δ and *CDC13 cgi121-*Δ *rad24-*Δ generated following dissection of the appropriate heterozygous diploid strain at 23°; see Figure S6 for the relative growth of these two strains at 30° and 36°.

mutation. Even at 23°, *cdc13-1* cells have reduced protein levels (Figure 4A) and thus presumably reduced *CDC13* activity, which is consistent with the synthetic lethality even at 23° that occurs when *cdc13-1* is combined with other telomere-specific mutations (Nugent *et al.* 1996; Polotnianka *et al.* 1998). Furthermore, Cdc13-1 protein levels (Figure 4A), as well as the ability of the mutant protein to associate with telomeres (Vodenicharov and Wellinger 2006), are unchanged following a shift to 36°. Given that the defect encoded by *cdc13-1* is so substantial that it is barely compatible with viability at 23°, we suggest that the combination of the *cdc13-1* mutation with the defect that gives rise to the Tmp$^-$ phenotype is responsible for inviability at 25°–26°. Although the Tmp$^-$ phenotype is most obvious at 34°–36° (where it affects the viability of telomerase- and Ku-defective strains), telomere length in wild-type cells is slightly reduced even at 30° relative to 23°. Furthermore, in *yku80-*Δ cells, the robust DNA damage response that occurs at 37° (as measured by autophosphorylation of Rad53) can also be detected at 30° although to a lesser degree (Teo and Jackson 2001). These observations are consistent with the idea that the Tmp$^-$ phenotype can confer a synthetic defect even at lower temperatures (as illustrated in Figure 9) in the presence of a severe mutation such as *cdc13-1*.

The Tmp$^-$ phenotype is potentially the basis for incorrectly assigning ts properties to hypomorphic mutations in *STN1* and *TEN1* as well. In the extensive panel of *stn1*$^-$ missense mutations reported here, every *stn1*$^-$ strain that exhibited a telomere length defect at 23° (corresponding to mutations in 24 amino acids) was accompanied by reduced

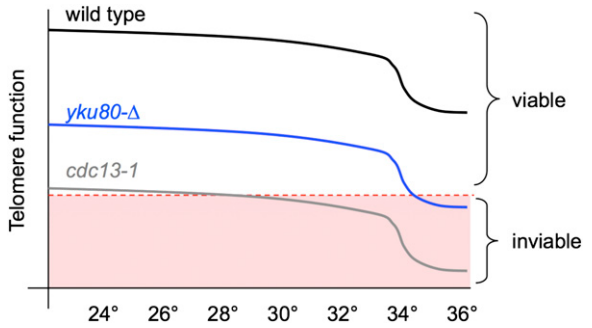

Figure 9 A schematic depiction of the additive contribution of the Tmp⁻ phenotype to the viability of strains bearing mutations in telomere-related proteins based on a decline in "telomere function" that occurs with increasing temperature. Since the molecular basis for the Tmp⁻ phenotype is unknown, telomere function is defined as "the collection of activities that maintain chromosome ends as fully replicated and capped telomeres."

viability at 34°–36°, a characteristic also displayed by the previously reported *stn1-13* and *stn1-63* mutant strains. This behavior is also similar to a recently reported panel of *ten1*⁻ mutations, which confer extremely elongated telomeres at permissive temperature, with growth impaired at 36° but not at lower temperatures (Xu *et al.* 2009). We suggest that these *ten1* alleles are also hypomorphs, rather than mutations that confer thermolabile Ten1 function. This suggestion also extends to a *stn1-td* degron construct that retains a significant degree of viability at 37° after switching on the degron (Vodenicharov and Wellinger 2006). Collectively, we propose that there are currently no *bona fide* *stn1*-ts or *ten1*-ts reagents that are wild type at permissive temperature and depleted for the essential function encoded by *STN1* or *TEN1* following a temperature shift.

Implications for analysis of telomere function at 36°

Although we were unsuccessful in our attempts to identify conditional lethal mutations in *STN1*, we did recover five new *cdc13-ts* alleles with nonpermissive temperatures between 30° and 33°. Unlike *cdc13-1*, these five mutations encode Cdc13 proteins that retain wild-type, or near wild-type, protein levels at 23° but are reduced by >10-fold at 36°. All five mutations map to the DNA-binding domain (Mitton-Fry *et al.* 2002), with three residues (S531, N609, and S611) in close physical proximity (data not shown). This suggests a region of the DBD that might be particularly prone to thermosensitive perturbations (alternatively, the recovery of mutations in these three residues may be simply a reflection of some bias in how the mutagenesis screens were conducted).

The identification of these new *cdc13-ts* strains allowed us to re-investigate a prior observation about the viability of Cdc13-depleted strains at nonpermissive temperatures. Previous experiments, which have monitored the viability of *cdc13-1 vs. cdc13-1 rad9*-Δ strains following prolonged incubation at 36° (Weinert and Hartwell 1993; Lydall and Weinert 1995), have concluded that loss of Cdc13 function creates structure(s) that, if left unrepaired, are lethal in the absence of Rad9 function (presumably as a consequence of unchecked cell-cycle progression). We re-examined this observation using a newly generated *cdc13-ts* allele (*cdc13-S611L*) that was nonpermissive for growth at 30° (Figure 5), which allowed us to compare the loss of viability in the absence of *RAD9* at 32°, 34°, and 36°. Even though 32° was fully nonpermissive for *CDC13* function, loss of viability was minimal. However, elevating the temperature to 34° or 36° resulted in a substantial further reduction in viability. Collectively, these observations suggest that, even in the absence of *RAD9*, loss of *CDC13* function does not lead to inviability *per se*. Instead, we propose that lethality is the consequence of an additional defect occurring at 34°–36°, when combined with *rad9*-Δ and *cdc13* depletion. If this proposal is correct, this suggests that hypotheses about the role of Cdc13 at telomeres as well as models derived from *cdc13-1*-induced DNA damage based on observations made at 34°–36° may need to be revisited, as the resulting phenotypes may be due to a more intricate set of genetic interactions than simply depletion of Cdc13. This point is further illustrated by the complex epistatic interaction that we observed between *cgi121*-Δ and *cdc13*-Δ mutations at different temperatures (Figure 8).

These results also have implications for genome-wide suppression and enhancer screens that have monitored viability of *cdc13-1* and *yku70*-Δ strains at temperatures ranging from 36° to 37.5° (Downey *et al.* 2006; Addinall *et al.* 2008, 2011). At least some subset of genes recovered from these screens is presumably due to a genetic interaction with the Tmp⁻ phenotype, rather than with either *CDC13* or *YKU70*. Although this does not negate the importance of these studies, the potential for such genes to further our understanding of telomere biology will require a fuller understanding of what telomeric process(es) are impaired by elevated temperature.

In addition, the impairment due to the reduction in Cdc13-1 protein levels suggests that a subset of genes recovered from such screens are involved in protein stability and/or turnover, rather than in telomere biology. This would explain how *STM1*, which modulates translation by regulating formation of the 80S subunit of ribosomes (Balagopal and Parker 2011), functions as a high copy suppressor of *cdc13-1* (Hayashi and Murakami 2002). Similarly, the recovery of *san1*-Δ as a robust suppressor of *cdc13-1* (Downey *et al.* 2006; Addinall *et al.* 2008) is consistent with a role for San1 in mediating degradation of misfolded nuclear proteins (Fredrickson *et al.* 2011). More generally, *cdc13-1* suppressors that are involved ribosome function, protein degradation, RNA processing, protein transport, and/or biosynthesis may have little direct relationship to telomere function.

What is the molecular basis for the Tmp⁻ phenotype?

This phenotype appears to be the consequence of a telomere-specific activity that is naturally temperature-labile even in wild-type cells, as evidenced by telomere shortening

at higher temperatures. This defect is presumably also responsible for the inviability observed in *yku70*-Δ and *yku80*-Δ strains, the enhanced senescence of telomerase-null strains, and the reduced microcolony growth of *RAD24*-deficient *cdc13*-Δ, *stn1*-Δ, and *ten1*-Δ null strains at 36°. Consistent with the premise that a common defect is responsible, the appearance of inviability in Ku-depleted cells exhibits phenotype lag (Barnes and Rio 1997). Similarly, the additive effect of temperature on telomerase-defective strains becomes more pronounced in later generations (Figure 2).

The temperature-induced inviability that occurs in *yku70*-Δ and *yku80*-Δ strains propagated at 36° has been characterized in detail by multiple laboratories, although with somewhat differing conclusions as to the molecular basis for the causative lesion (Fellerhoff *et al.* 2000; Teo and Jackson 2001; Gravel and Wellinger 2002; Maringele and Lydall 2002; Smith *et al.* 2008). Several studies have lent support to the idea that an altered terminal DNA structure, which is generated when telomeres fall below a minimal length, is responsible. The shortening rate at 36° in Ku-depleted cells is inconsistent with a telomerase defect (Gravel and Wellinger 2002), which is also supported by our results indicating that the temperature-dependent reduction in telomere length is not due to an impaired ability of telomerase at 36°. These observations therefore argue for an active shortening mechanism that occurs at high temperature. In the absence of Ku function, telomere-proximal regions replicate early (Cosgrove *et al.* 2002; Lian *et al.* 2011). If high temperature further exacerbates this altered replication timing profile (*e.g.*, as a consequence of the shorter cell-cycle time at 36°), we suggest that this could lead to incomplete replication of the duplex telomeric DNA tract by the conventional DNA replication machinery and hence to telomere shortening.

Regardless of the molecular defect that underlies the Tmp$^-$ phenotype, this telomere-specific response is just one aspect of a pleiotrophic set of responses by cells to higher temperatures. Cells have a well-orchestrated mechanism for response to temperature fluctuations. Thus, other cellular pathways may also experience an analogous version of the Tmp$^-$ phenotype. The results described here also raise a cautionary note about using phenotypic analysis as the sole basis for categorizing ts mutations. This suggests that efforts to create genome-wide epistasis maps using a comprehensive array of temperature-sensitive reagents may need to take this into account (Ben-Aroya *et al.* 2008; Li *et al.* 2011).

Acknowledgments

We thank Madeleine Jennewein and Monika Walterscheid who each contributed to the initial stages of one of the forward mutagenesis *cdc13-ts* screens; Edward K. Mandell for conducting the Evolutionary Trace analysis on Cdc13; and other members of the Lundblad laboratory for many helpful discussions during the course of this work. This research was supported by grant GM55867 and Cancer Center Core grant P30-CA014195 from the National Institutes of Health and by funding from the F. M. Kirby Foundation, the G. Harold and Leila Y. Mathers Charitable Foundation, and the Chapman Foundation.

Literature Cited

Addinall, S. G., M. Downey, M. Yu, M. K. Zubko, J. Dewar *et al.*, 2008 A genomewide suppressor and enhancer analysis of *cdc13–1* reveals varied cellular processes influencing telomere capping in *Saccharomyces cerevisiae*. Genetics 180: 2251–2266.

Addinall, S. G., E. M. Holstein, C. Lawless, M. Yu, K. Chapman *et al.*, 2011 Quantitative fitness analysis shows that NMD proteins and many other protein complexes suppress or enhance distinct telomere cap defects. PLoS Genet. 7: e1001362.

Askree, S. H., T. Yehuda, S. Smolikov, R. Gurevich, J. Hawk *et al.*, 2004 A genome-wide screen for *Saccharomyces cerevisiae* deletion mutants that affect telomere length. Proc. Natl. Acad. Sci. USA 101: 8658–8663.

Balagopal, V., and R. Parker, 2011 Stm1 modulates translation after 80S formation in *Saccharomyces cerevisiae*. RNA 17: 835–842.

Barnes, G., and D. Rio, 1997 DNA double-strand-break sensitivity, DNA replication, and cell cycle arrest phenotypes of Ku-deficient *Saccharomyces cerevisiae*. Proc. Natl. Acad. Sci. USA 94: 867–872.

Ben-Aroya, S., C. Coombes, T. Kwok, K. A. O'Donnell, J. D. Boeke *et al.*, 2008 Toward a comprehensive temperature-sensitive mutant repository of the essential genes of *Saccharomyces cerevisiae*. Mol. Cell 30: 248–258.

Bertuch, A. A., and V. Lundblad, 2003 The Ku heterodimer performs separable activities at double-strand breaks and chromosome termini. Mol. Cell. Biol. 23: 8202–8215.

Boulton, S. J., and S. P. Jackson, 1996 Identification of a *Saccharomyces cerevisiae* Ku80 homologue: roles in DNA double strand break rejoining and in telomeric maintenance. Nucleic Acids Res. 24: 4639–4648.

Carson, M., and L. Hartwell, 1985 *CDC17*: an essential gene that prevents telomere elongation in yeast. Cell 42: 249–257.

Chandra, A., T. R. Hughes, C. I. Nugent, and V. Lundblad, 2001 Cdc13 both positively and negatively regulates telomere replication. Genes Dev. 15: 404–414.

Cosgrove, A. J., C. A. Nieduszynski, and A. D. Donaldson, 2002 Ku complex controls the replication time of DNA in telomere regions. Genes Dev. 16: 2485–2490.

Downey, M., R. Houlsworth, L. Maringele, A. Rollie, M. Brehme *et al.*, 2006 A genome-wide screen identifies the evolutionarily conserved KEOPS complex as a telomere regulator. Cell 124: 1155–1168.

Feldmann, H., and E. L. Winnacker, 1993 A putative homolgue of the human autoantigen Ku from *Saccharomyces cerevisiae*. J. Biol. Chem. 268: 12895–12900.

Feldmann, H., L. Driller, B. Meier, G. Mages, J. Kellermann *et al.*, 1996 *HDF2*, the second subunit of the Ku homologue from *Saccharomyces cerevisiae*. J. Biol. Chem. 271: 27765–27769.

Fellerhoff, B., F. Eckardt-Schupp, and A. A. Friedl, 2000 Subtelomeric repeat amplification is associated with growth at elevated temperature in *yku70* mutants of *Saccharomyces cerevisiae*. Genetics 154: 1039–1051.

Fredrickson, E. K., J. C. Rosenbaum, M. N. Locke, T. I. Milac, and R. G. Gardner, 2011 Exposed hydrophobicity is a key determinant of nuclear quality control degradation. Mol. Biol. Cell 22: 2384–2395.

Gao, H., R. B. Cervantes, E. K. Mandell, J. H. Otero, and V. Lundblad, 2007 RPA-like proteins mediate yeast telomere function. Nat. Struct. Mol. Biol. 14: 208–214.

Gao, H., T. B. Toro, M. Paschini, B. Braunstein-Ballew, R. B. Cervantes *et al.*, 2010 Telomerase recruitment in *Saccharomyces cerevisiae* is not dependent on Tel1-mediated phosphorylation of Cdc13. Genetics 186: 1147–1159.

Gatbonton, T., M. Imbesi, M. Nelson, J. M. Akey, D. M. Ruderfer *et al.*, 2006 Telomere length as a quantitative trait: genome-wide survey and genetic mapping of telomere length-control genes in yeast. PLoS Genet. 2: e35.

Grandin, N., and M. Charbonneau, 2001 Hsp90 levels affect telomere length in yeast. Mol. Genet. Genomics 265: 126–134.

Grandin, N., S. I. Reed, and M. Charbonneau, 1997 Stn1, a new *Saccharomyces cerevisiae* protein, is implicated in telomere size regulation in association with Cdc13. Genes Dev. 11: 512–527.

Grandin, N., C. Damon, and M. Charbonneau, 2001 Ten1 functions in telomere end protection and length regulation in association with Stn1 and Cdc13. EMBO J. 20: 1173–1183.

Gravel, S., and R. J. Wellinger, 2002 Maintenance of double-stranded telomeric repeats as the critical determinant for cell viability in yeast cells lacking Ku. Mol. Cell. Biol. 22: 2182–2193.

Hayashi, N., and S. Murakami, 2002 *STM1*, a gene which encodes a guanine quadruplex binding protein, interacts with *CDC13* in *Saccharomyces cerevisiae*. Mol. Genet. Genomics 267: 806–813.

Lendvay, T. S., D. K. Morris, J. Sah, B. Balasubramanian, and V. Lundblad, 1996 Senescence mutants of *Saccharomyces cerevisiae* with a defect in telomere replication identify three additional *EST* genes. Genetics 144: 1399–1412.

Li, Z., F. J. Vizeacoumar, S. Bahr, J. Li, J. Warringer *et al.*, 2011 Systematic exploration of essential yeast gene function with temperature-sensitive mutants. Nat. Biotechnol. 29: 361–367.

Lian, H. Y., E. D. Robertson, S. Hiraga, G. M. Alvino, D. Collingwood *et al.*, 2011 The effect of Ku on telomere replication time is mediated by telomere length but is independent of histone tail acetylation. Mol. Biol. Cell 22: 1753–1765.

Lichtarge, O., and M. E. Sowa, 2002 Evolutionary predictions of binding surfaces and interactions. Curr. Opin. Struct. Biol. 12: 21–27.

Lichtarge, O., H. R. Bourne, and F. E. Cohen, 1996 An evolutionary trace method defines binding surfaces common to protein families. J. Mol. Biol. 257: 342–358.

Lundblad, V., and J. W. Szostak, 1989 A mutant with a defect in telomere elongation leads to senescence in yeast. Cell 57: 633–643.

Lustig, A. J., and T. D. Petes, 1986 Identification of yeast mutants with altered telomere structure. Proc. Natl. Acad. Sci. USA 83: 1398–1402.

Lydall, D., and T. Weinert, 1995 Yeast checkpoint genes in DNA damage processing: implications for repair and arrest. Science 270: 1488–1491.

Maringele, L., and D. Lydall, 2002 ExoI-dependent single-stranded DNA at telomeres activates subsets of DNA damage and spindle checkpoint pathways in budding yeast *yku70*Δ mutants. Genes Dev. 16: 1919–1933.

Mitton-Fry, R. M., E. M. Anderson, T. R. Hughes, V. Lundblad, and D. S. Wuttke, 2002 Conserved structure for single-stranded telomeric DNA recognition. Science 296: 145–147.

Nugent, C. I., T. R. Hughes, N. F. Lue, and V. Lundblad, 1996 Cdc13p: a single-strand telomeric DNA-binding protein with a dual role in yeast telomere maintenance. Science 274: 249–252.

Paschini, M., E. K. Mandell, and V. Lundblad, 2010 Structure prediction-driven genetics in *Saccharomyces cerevisiae* identifies an interface between the t-RPA proteins Stn1 and Ten1. Genetics 185: 11–21.

Paulovich, A. G., R. U. Margulies, B. M. Garvik, and L. H. Hartwell, 1997 *RAD9*, *RAD17*, and *RAD24* are required for S phase regulation in *Saccharomyces cerevisiae* in response to DNA damage. Genetics 145: 45–62.

Polotnianka, R. M., J. Li, and A. J. Lustig, 1998 The yeast Ku heterodimer is essential for protection of the telomere against nucleolytic and recombinational activities. Curr. Biol. 8: 831–834.

Puglisi, A., A. Bianchi, L. Lemmens, P. Damay, and D. Shore, 2008 Distinct roles for yeast Stn1 in telomere capping and telomerase inhibition. EMBO J. 27: 2328–2339.

Rizki, A., and V. Lundblad, 2001 Defects in mismatch repair promote telomerase-independent proliferation. Nature 411: 713–716.

Shampay, J., J. W. Szostak, and E. H. Blackburn, 1984 DNA sequences of telomeres maintained in yeast. Nature 310: 154–157.

Small, V. Y., C. Chuang, and C. I. Nugent, 2008 Rad24 truncation, coupled with altered telomere structure, promotes *cdc13–1* suppression in *S. cerevisiae*. Cell Cycle 7: 3428–3439.

Smith, S., S. Banerjee, R. Rilo, and K. Myung, 2008 Dynamic regulation of single-stranded telomeres in *Saccharomyces cerevisiae*. Genetics 178: 693–701.

Szostak, J. W., and E. H. Blackburn, 1982 Cloning yeast telomeres on linear plasmid vectors. Cell 29: 245–255.

Teo, S. H., and S. P. Jackson, 2001 Telomerase subunit overexpression suppresses telomere-specific checkpoint activation in the yeast *yku80* mutant. EMBO Rep. 2: 197–202.

Vodenicharov, M. D., and R. J. Wellinger, 2006 DNA degradation at unprotected telomeres in yeast is regulated by the CDK1 (CDC28/Clb) cell cycle kinase. Mol. Cell 24: 127–137.

Weinert, T. A., and L. H. Hartwell, 1993 Cell cycle arrest of *cdc* mutants and specificity of the *RAD9* checkpoint. Genetics 134: 63–80.

Weinert, T. A., G. L. Kiser, and L. H. Hartwell, 1994 Mitotic checkpoint genes in budding yeast and the dependence of mitosis on DNA replication and repair. Genes Dev. 8: 652–665.

Xu, L., R. C. Petreaca, H. J. Gasparyan, S. Vu, and C. I. Nugent, 2009 *TEN1* is essential for *CDC13*-mediated telomere capping. Genetics 183: 793–810.

Communicating editor: J. Sekelsky

GENETICS

Supporting Information
http://www.genetics.org/content/suppl/2012/02/28/genetics.111.137869.DC1

A Naturally Thermolabile Activity Compromises Genetic Analysis of Telomere Function in *Saccharomyces cerevisiae*

Margherita Paschini, Tasha B. Toro, Johnathan W. Lubin, Bari Braunstein-Ballew, Danna K. Morris, and Victoria Lundblad

DOI: 10.1534/genetics.111.137869

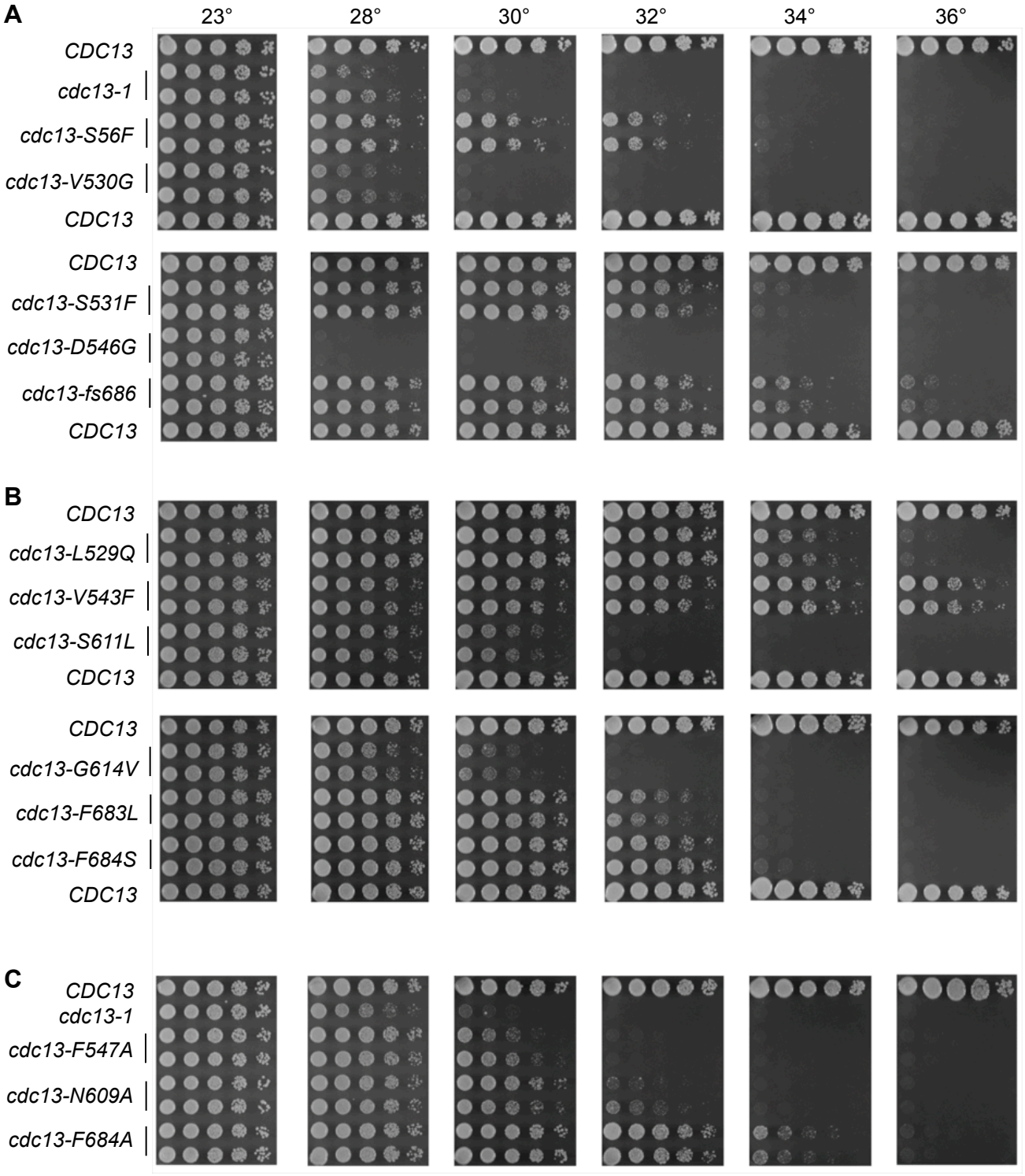

Figure S1 Identification of new *cdc13-ts* mutations, part I. Mutant alleles recovered from (A) forward mutagenesis of the full length *CDC13* gene, (B) forward mutagenesis directed at the DBD of *CDC13* or (C) reverse mutagenesis of the DBD of *CDC13* were transformed into a *cdc13-Δ/* p*CEN CDC13 URA3* shuffle strain and subsequently streaked on 5-FOA media at 23°, to recover isolates which had lost the wild type *CDC13* plasmid. The resulting strains were grown overnight in culture and viability was assessed by plating serial dilutions on pre-warmed rich media plates and photographing after 2.5 days (for ≥ 28° incubations) or 4 days (for 23° and 25°).

A

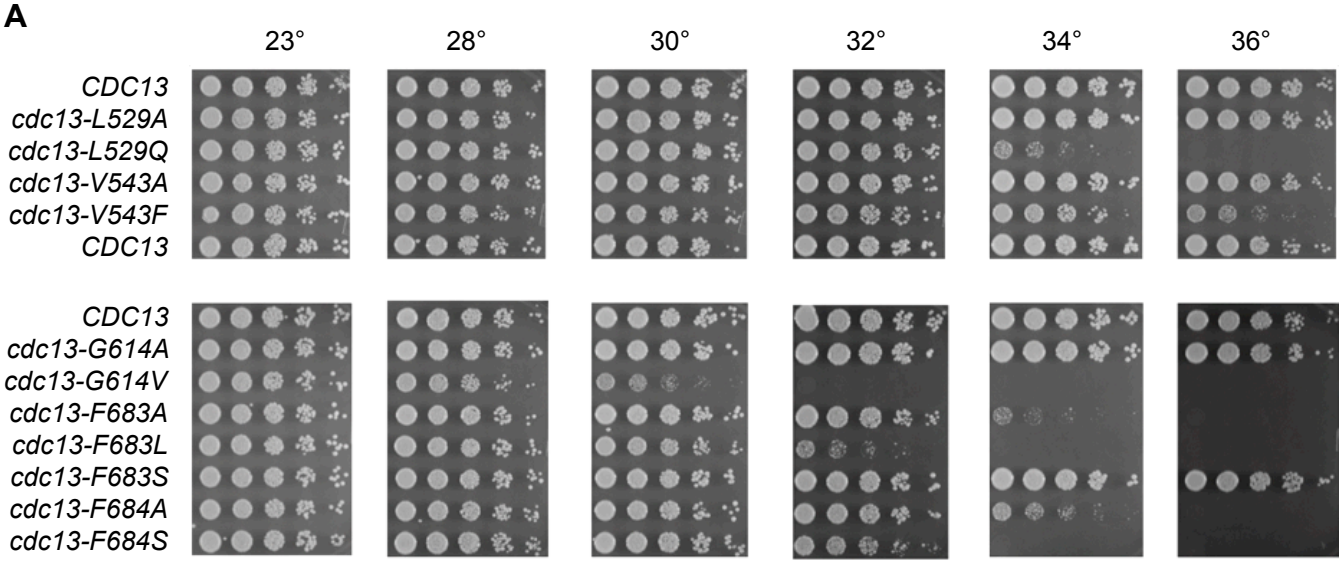

B

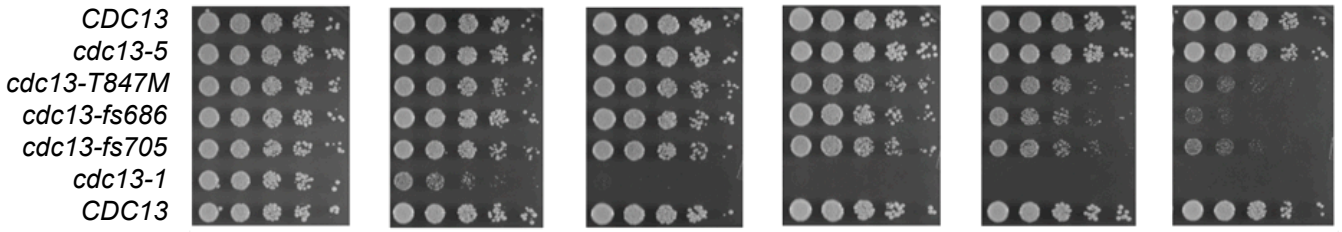

C

Allele	Mutations present (**cluster 1**, **cluster 2**, **cluster 3**)
isolate 22	**V543F**
isolate 23	N609D
isolate 26	N609D, Y626F
isolate 19	L599P, S650P
isolate 16	**M525T**, I633V
isolate 30	T507A, **L529Q**
isolate 21	**S533L**, **V616A**
isolate 15	M463I, **S611L**
isolate 31	P506S, **G614V**
isolate 28	**K618E**, **F683S**
isolate 20	N631D, **F684S**
isolate 17	**D535G**, P651L, **F683L**
isolate 24	V481E, A489T, L562Q
isolate 25	T496S, E519V, I578T
isolate 27	F575L, N627S, Y680C, **I686V**
isolate 29	M498V, **F544L**,T586M, K629E
isolate 18	**S531T**, I563V, E608V, K629E, L693P
isolate 14	N455D, T473A, D492G, I552T, F574S

Figure S2 Identification of new *cdc13-ts* mutations, Part II. (A) Additional mutant alleles, as discussed in the text, were analyzed as described in Figure S1. (B) Missense mutations identified in a panel of *cdc13-ts* alleles, following mutagenesis of the DNA binding domain with error-prone PCR, remissense; clusters of residues discussed in the text are indicated.

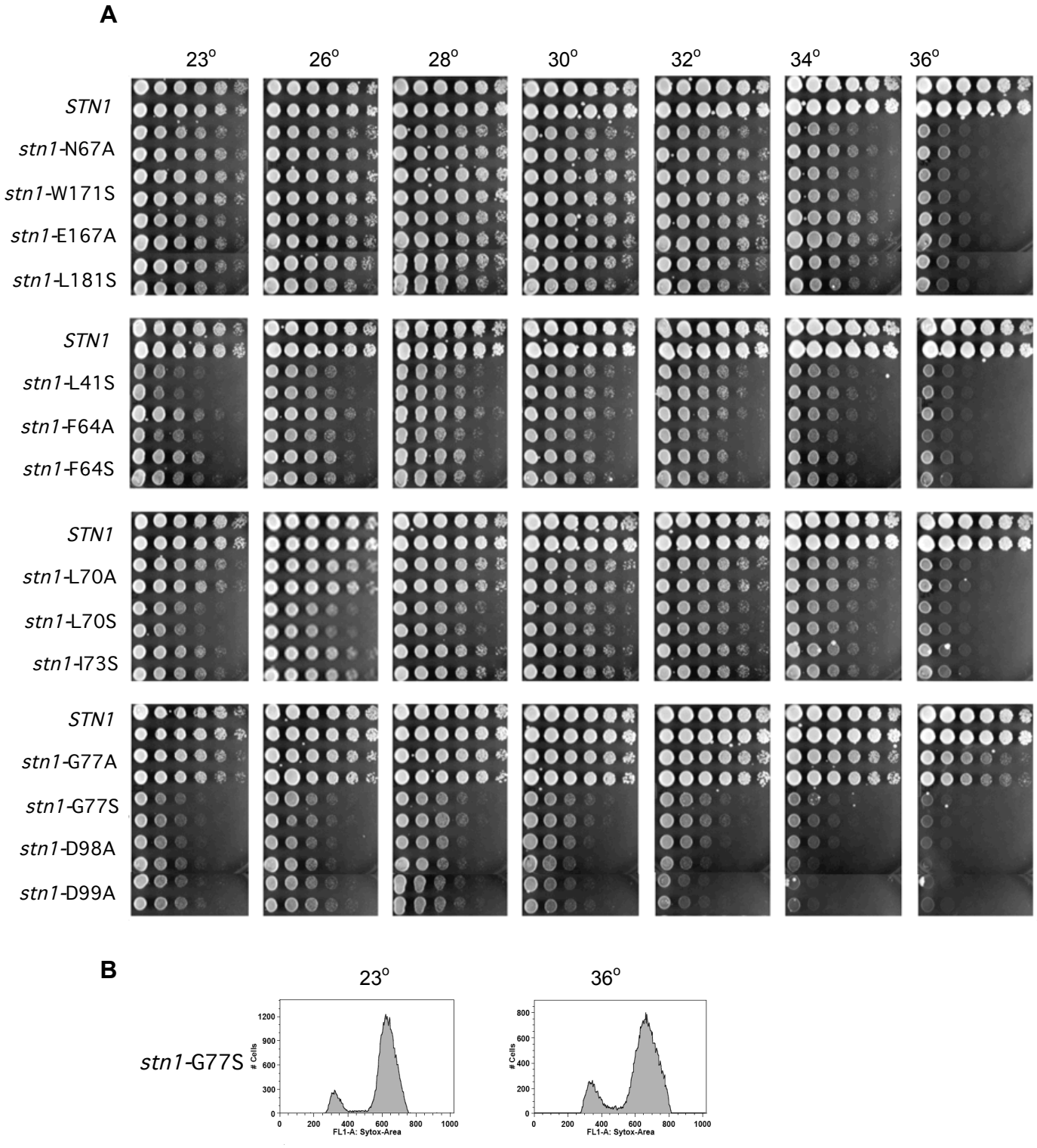

Figure S3 Viability assays of *stn1*¯ missense mutations. (A) Plasmids carrying the indicated *Stn1* alleles were transformed into a *stn1-Δ/* p*CEN STN1 URA3* shuffle strain and subsequently streaked on 5-FOA media at 23°, to recover isolates which had lost the wild type *STN1* plasmid. The resulting strains were grown overnight in culture and viability was assessed by plating serial dilutions of two isolates for each genotype on pre-warmed rich media plates and photographing after 2.5 days (for ≥ 28° incubations) or 4 days (for 23° and 25°). (B) Flow cytometry profile of log-phase cultures of a *stn1-Δ*/p *stn1-G77S* strain grown at 23° and 36° for 3.5h.

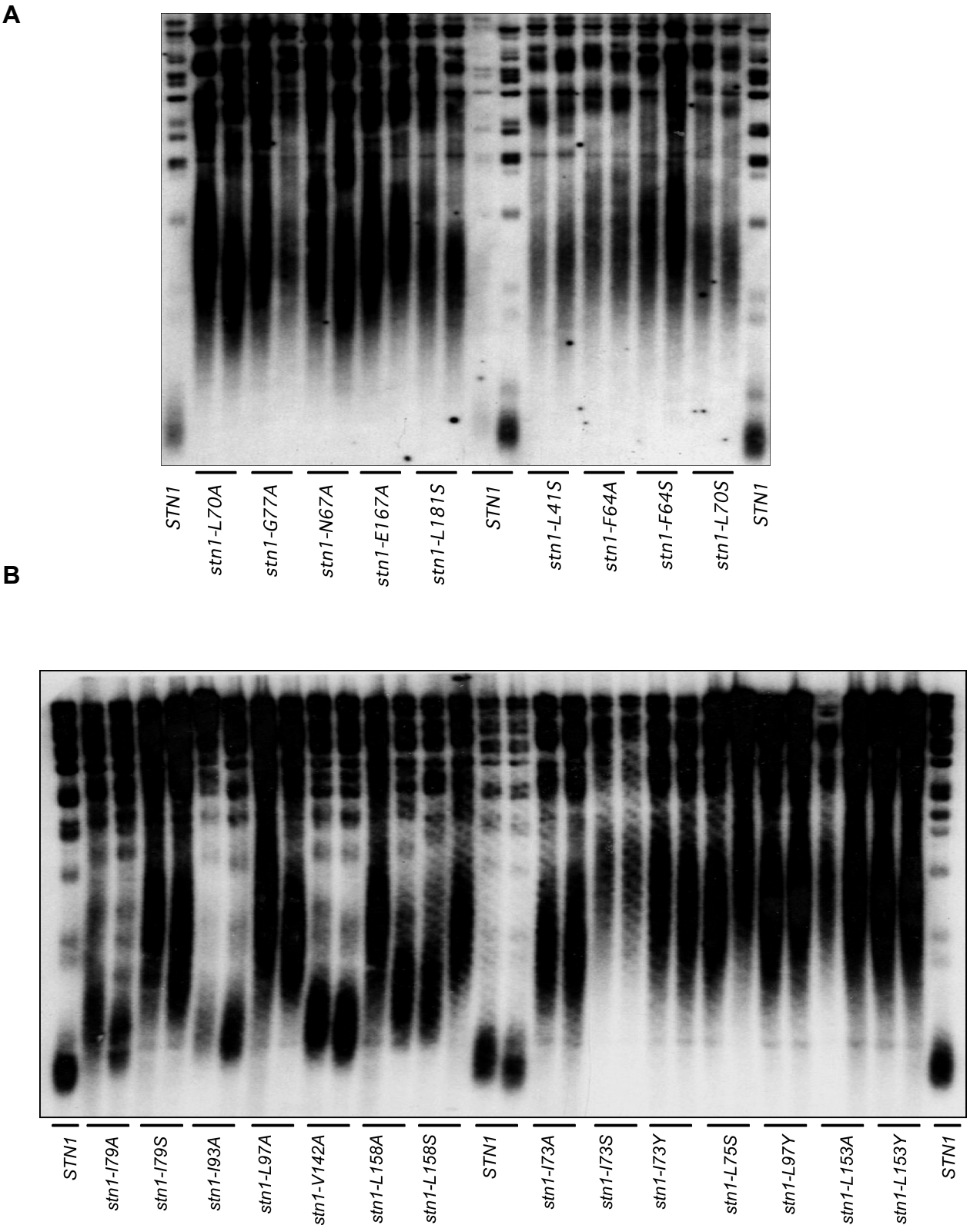

Figure S4 Telomere length of strains expressing *stn1*$^{-}$ missense mutations in residues selected for reverse mutagenesis based on either (A) Evolutionary Trace or (B) position of the side-chain relative to the interior of the β-barrel of the essential N-terminal OB-fold domain of Stn1; *stn1-Δ* strains with *CEN* plasmids expressing the indicated mutations were grown at 23° prior to preparing genomic DNA for telomere length analysis.

	Viable?	Telomere length	23°	36°
I73A		Very long	+	+/-
I73S	Nearly inviable	Extremely long	+/-	—
I73Y		Very long	+	+/- to (+)
L75A		Med long	+	(+) to +
L75S		Very long	(+) to +	+/- to (+)
L75Y	inviable	n/a		
I79A		Med long	++	+
I79S		Very long	+ to ++	(+)
I79Y	inviable	n/a		
I93A		Med long	++	+
I93S		Very long	+	+/- to (+)
I93Y		Slightly long	++	+
L97A		Very long	(+)	+/-
L97S	inviable	n/a		
L97Y		Very long	(+) to +	+/-
L106A		Wild type	++	++
L106S		Wild type	++	++
L106Y		Wild type	++	++
L140A		Wild type	++	++
L140S		Wild type	++	++
L140Y		Wild type	++	++
V142A		Slightly long	+ to ++	+
V142S	Nearly inviable	n.t.	+/-	—
V142Y	inviable	n/a		
L153A		Very long	(+)	+/-
L153S	inviable	n/a		
L153Y		Very long	(+)	+/-
V155A		Very long	+	(+)
V155S	Nearly inviable	n.t.	+/-	—
V155Y	inviable	n/a		
L158A		Very long	+	+
L158S		Very long	+	+
L158Y		n.t.	(+)	+/-
G77A		Very long	(+) to +	+/- to +
G77S		n.t.	(+)	+/-
G77Y	Nearly inviable	n.t.	+/-	—
G137A	+	Very long	+(+)	(+)
G137S	+	Long	++	+
G137Y	inviable	n/a		

Figure S5 Summary of viability and telomere length of a panel of *stn1*⁻ missense mutations introduced into 11 hydrophobic residues with side-chains located in the interior of the β-barrel of the essential N-terminal OB-fold domain of Stn1. Telomere length of selected mutant isolates is shown in Figure S4. The results for mutagenesis of two highly conserved glycine residues are also included.

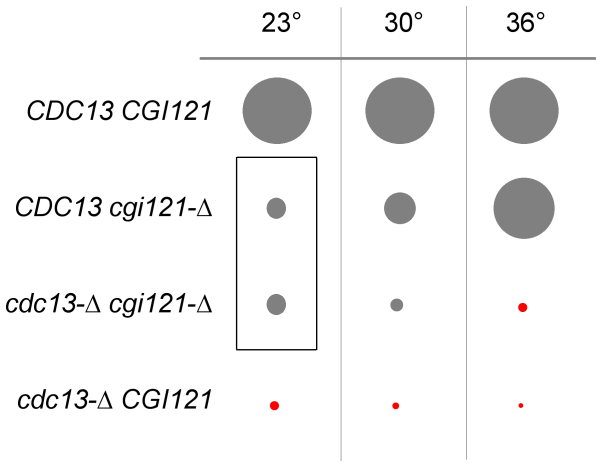

Figure S6 Schematic of relative colony size following dissection of a *CDC13/cdc13-Δ RAD24/rad24-Δ CGI121/cgi121-Δ* diploid; colony size is roughly to scale, with red dots indicating colonies that can only visulized with magnification. All indicated genoytpes are also *rad24-Δ.* Data for representative colonies indicated by the box are shown in Figure 8C.